

Supporting Information

**Formation and Evolution of Molecular Products in α -Pinene
Secondary Organic Aerosol**

Xuan Zhang^a, Renee C. McVay^b, Dan D. Huang^c, Nathan F. Dalleska^a,
Bernard Aumont^d, Richard C. Flagan^{a,b}, John H. Seinfeld^{a,b}

^a Division of Engineering and Applied Science, California Institute of Technology, Pasadena, CA 91125, USA

^b Division of Chemistry and Chemical Engineering, California Institute of Technology, Pasadena, CA 91125, USA

^c Department of Chemical and Biomolecular Engineering, Hong Kong University of Science and Technology, Hong Kong, China

^d Laboratoire Interuniversitaire des Systèmes Atmosphériques (LISA), UMR CNRS 7583, Université Paris Est Créteil et Université Paris Diderot, 94010 Créteil, France

To whom correspondence should be addressed: seinfeld@caltech.edu

This file includes:

S1. Chamber Experiments

S2. Instrument Operation and Data Analysis Protocols

S2.1 Chemical Ionization Mass Spectrometer (CIMS)

S2.2 Scanning Mobility Particle Sizer (SMPS)

S2.3 Aerosol Mass Spectrometer (AMS)

S2.4 Particle-into-Liquid Sampler (PILS)

S2.5 Ultra Performance Liquid Chromatography / Electrospray Ionization Quadrupole Time-of-Flight Mass Spectrometry (UPLC/ESI-Q-ToFMS)

S3. Characterization of Monomers and Dimers in α -pinene SOA

S3.1 Molecular Structure elucidation

S3.2 Quantification

S3.2.1 Particle-Phase Components Mass Concentration Retrieval

S3.2.2 Electrospray Ionization Efficiency Estimation

S3.2.3 Uncertainty Analysis

S4. Vapor-Particle Dynamics Model

References

Figures S1 to S10

Tables S1 to S4

S1. Chamber Experiments

α -pinene SOA formation experiments were conducted in the Caltech dual 24-m³ Environmental Chamber, in which the temperature (T) and relative humidity (RH) are automatically controlled. Prior to each experiment, the Teflon chambers were flushed with purified, dry air for 24 h until the particle number concentration $< 10 \text{ cm}^{-3}$ and volume concentration $< 0.01 \text{ }\mu\text{m}^3 \text{ cm}^{-3}$. For humid experiments, the Teflon chamber was humidified to $\sim 50\%$ by passing purified air through a Nafion membrane humidifier (FC200, Permapure LLC) that is kept wet by recirculation of 27 °C ultra-pure water (18 M Ω , Millipore Milli-Q). Seed aerosols were injected into the chamber by atomizing 0.015 M aqueous ammonium sulfate (AS) solution to provide sufficient surface area for partition of products. For humid experiments, a custom-built wet-wall denuder was employed to generate hydrated ammonium sulfate seed aerosol. 15 μL α -pinene (Sigma-Aldrich, 98% purity) was injected into a glass bulb, which was connected into the Teflon chamber via a 1/4" O.D. Teflon tubing. Heated 5 L min⁻¹ of purified, dry air flowed through the glass bulb into the chamber for 30 min, introducing ~ 150 ppb α -pinene into the chamber. For dark ozonolysis experiments, O₃ was introduced into the chamber by flowing 5 L min⁻¹ dry, purified air through an ozone generator (EMMET). For photooxidation experiments, hydrogen peroxide (H₂O₂) was used for the OH source by evaporating 113 μL of 50 wt % aqueous solution into the chamber with 5 L min⁻¹ purified air for ~ 110 min, resulting in an approximate starting H₂O₂ mixing ratio of 2 ppm. After ~ 1 h mixing, photooxidation was initiated by irradiating the chamber with black lights with output wavelength ranging from 300 to 400 nm.

Relative Humidity and temperature were monitored via a Vaisala HMM211 probe. O₃ and NO_x mixing ratios were measured by a Horiba O₃ analyzer (APOA-360) and a Teledyne NO_x analyzer (T200), respectively. α -pinene concentration was monitored by a gas chromatograph equipped with a HP-5 column (15 m \times 0.53 mm ID \times 1.5 μm thickness, Hewlett-Packard) coupled with flame ionization detector (GC/FID, Agilent 6890N). In addition, a suite of instruments was used to investigate gas- and particle-phase chemistry, see Section S2.

S2. Instrument Operation and Data Analysis Protocols

S2.1 Chemical Ionization Mass Spectrometer (CIMS)

The gas-phase products from α -pinene+O₃/OH reaction were monitored using a custom-modified Varian 1200 triple-quadrupole Chemical Ionization Mass Spectrometer (CIMS). In negative mode operation, CF₃O⁻ was used as the reagent ion to cluster with an analyte such as hydroperoxide or acid [R], producing [R·CF₃O]⁻ or m/z [M+85]⁻, where M is the molecular weight of the analyte. For more strongly acidic species [H·X], the transfer product, [H·X·F]⁻ or m/z [M+19]⁻, is formed during ionization. Carboxylic acids tend to have contributions to both the transfer and cluster product, in which case the overall signal of a compound is considered as the sum of the two product signals.

S2.2 Scanning Mobility Particle Sizer (SMPS)

The size distribution and number concentration of seed particles and organic aerosols were characterized using a custom-built Scanning Mobility Particle Sizer (SMPS) consisting of a Differential Mobility Analyzer (DMA, TSI, 3081) coupled with a Condensation Particle Counter (CPC, TSI, 3010). The DMA was operated in a closed system with a recirculating sheath and excess flow of 2.67 L min⁻¹ and a 5.4 : 1 ratio of sheath to aerosol flow rate. The column voltage was scanned from 15 to 9850 V over 45 s. More details on the SMPS operation are given by Loza et al. (1) and Zhang et al. (2). Particle wall loss is not accounted for in the derivation of the overall SOA volume and mass, in order to directly compare with the mass concentration of individual products detected in the suspended particles in the chamber. For a typical ozonolysis experiment conducted at 298 K and < 5% RH, the initial AS seed volume is ~70 $\mu\text{m}^3 \text{cm}^{-3}$, and the initial AS seed number distribution spans from ~20 nm to ~600 nm, with a median diameter of ~80 nm. Growth driven by gas-phase chemistry and gas-particle partitioning occurs primarily on large particles and, as a result, the number median diameter shifts to ~200 nm after ~5 h of reaction.

S2.3 Aerosol Mass Spectrometer (AMS)

Real-time particle mass spectra were collected continuously by an Aerodyne High Resolution Time-of-Flight Aerosol Mass Spectrometer (AMS). All AMS data were

processed with “Squirrel”, the ToF-AMS Unit Resolution Analysis Toolkit (<http://cires.colorado.edu/jimenez-group/ToFAMSResources/ToFSoftware/index.html>), in Igor Pro Version 6.36 (Wavemetrics, Lake Oswego, OR). The ToF-AMS High Resolution Analysis software tool PIKA (Peak Integration by Key Analysis) was employed for high-resolution analysis. Interference of chamber air on the particulate spectrum was corrected by adjusting parameters in the fragmentation table based on the “filter run” (AMS is collecting chamber air with a particle filter in-line) before each experiment. The Improved-Ambient method has been updated in the elemental ratio calculation algorithm (3). The derived average O:C ratios of SOA from α -pinene+O₃ reaction at 298K and < 5% RH range from ~0.45 to ~0.50, which is ~50% higher than that estimated by the traditional routine (4).

S2.4 Particle-into-Liquid Sampler (PILS)

Chamber generated α -pinene SOA was sampled through a 1 μm cut size impactor with a flow rate of 12.5 L min⁻¹, and passed successively through individual acid and base gas denuders and an organic carbon denuder to remove inorganic and organic vapors. A steam flow generated at 100 °C is adiabatically mixed with the cooler aerosol flow in a condensation chamber, creating a high water supersaturation environment in which particles grow sufficiently large ($D_p > 1 \mu\text{m}$) for collection by inertial impaction onto a quartz plate. Impacted particles are transported to a debubbler by a washing flow (0.15 mL min⁻¹) comprising 50% water and 50% isopropanol. The sampled liquid is delivered into vials held on a rotating carousel. Under the current configuration, a 5-min time resolution can be achieved for the characterization of particle-phase dynamics. In this way, a total of 72 liquid samples were collected for an experiment with approximately 6 h duration.

S2.5 Ultra Performance Liquid Chromatography / Electrospray Ionization Quadrupole Time-of-Flight Mass Spectrometry (UPLC/ESI-Q-ToFMS)

PILS collected liquid samples were analyzed by a WATERS ACQUITY UPLC I-Class System, coupled with a Quadrupole Time-of-Flight Mass Spectrometer (Xevo G2-S QToF) and equipped with an Electrospray Ionization (ESI) source. Sample temperature was kept at 4 °C. An ACQUITY BEH C₁₈ column (2.1 × 50 mm) was used to separate the

particle-phase product generated from α -pinene reaction with OH/O₃. The 12-min eluent program is: (0 – 2.0 min) 100% A (0.1% v/v formic acid in 99% v/v water and 1% v/v acetonitrile); (2.0 – 10.2 min) 10% A and 90% B (acetonitrile); and (10.2 – 12 min) 100% A. The total flow rate is 0.3 mL min⁻¹ and the injection volume is 10 μ L. The column temperature was kept at 30 °C. Optimum electrospray conditions are: 2.0 kV capillary voltage, 40 V sampling cone, 80 V source offset, 120 °C source temperature, 500 °C desolvation temperature, 30 L h⁻¹ cone gas, and 650 L h⁻¹ desolvation gas. Negative ion mass spectra were acquired over a mass range of 40 – 1000 Da. MS/MS spectra were obtained by applying a collision energy ramping program starting from 15 eV to 50 eV over one MS scan in the collision cell. Accurate masses were corrected by a lock spray of leucine enkephalin (m/z 556.2771 [M+H]⁺). Data were acquired and processed using the MassLynx v4.1 software.

S3. Characterization of Monomers and Dimers in α -pinene SOA

S3.1 Molecular Structure Elucidation

SI Appendix, Figure S1 (A–C) shows the UPLC/(–)ESI-Q-ToFMS base peak chromatograms (BPCs) for the PILS collected SOA sample (5-min duration) when > 99% α -pinene is consumed via reaction with O₃ at 298 K + 5% RH, 298 K + 50% RH, and 285 K + 5% RH respectively. The dominant ions include m/z 213 (retention time, RT 3.81 min), m/z 197 (RT 3.86 min), m/z 171 (RT 3.96 min), m/z 199 (RT 4.07 min), m/z 185 (RT 4.35 min), m/z 357 (RT 5.32 min), m/z 299 (RT 5.78 min) and m/z 367 (RT 5.98 min). They are produced in the negative mode of electrospray ionization by the loss of a hydrogen atom from the parent molecule ([M–H][–]). The ions at m/z 171, m/z 185, m/z 197, and m/z 199 appear in the BPCs of SOA samples generated from the OH-initiated oxidation of α -pinene as well, see *SI Appendix, Figure S1 (D)*, whereas ions at higher mass-to-charge ratio (m/z 213, m/z 299, m/z 357, and m/z 367) were not observed over the course of the photooxidation experiment. In addition to the ions that are apparently present on the BPCs, a series of less abundant ions with the mass-to-charge ratio ranging from ~150 to ~400 were also characterized, as listed in *SI Appendix, Table S2*. It is worth noting that each ion we present here has a distinct retention time due to its unique

interactions with the LC column, thus confirming that they are actual α -pinene SOA products instead of artifacts generated in the ESI process.

Molecular structure elucidation of each ion listed in *SI Appendix, Table S2* is based on the first-order (–) ESI mass spectra and fragmentation characteristics in the MS/MS spectra. *SI Appendix, Figure S2* shows the extracted ion chromatograph (EIC), as well as (–) ESI MS and MS/MS spectra for each ion. The major peak on the m/z 183 (RT 4.96 min) EIC is assigned to pinonic acid based on comparison of its chromatographic and mass spectrometric behavior with that of commercial available standard *cis*-pinonic acid (Sigma-Aldrich, 98% purity). The MS/MS product spectrum of m/z 183 reveals a major peak at m/z 139 due to the neutral loss of CO_2 (44 u), see *SI Appendix, Figure S2 (H)*. Similar fragmentation patterns were also observed for ions at m/z 169, 171, 185, 189, 197, and 199, as shown in *SI Appendix, Figure S2 (G3, C3, F3, A3, B3, and D3)*. They are assigned to pinalic acid, terpenylic acid, pinic acid, diaterpenylic acid, oxopinonic acid, and hydroxypinonic acid, respectively, consistent with previous studies (5-15). Note that neutral loss of CO_2 has been demonstrated as an abundant dissociation pathway of deprotonated carboxylic acid upon collision induced dissociation (16). The m/z 171 EIC shows a dominant peak at retention time (RT) 3.96 min, which is assigned to terpenylic acid, as well as a small shoulder peak at RT 4.07 min, which is assigned to norpinic acid, based on comparison with LC/MS data reported in literature (12). The major peak in the m/z 199 EIC is attributed to hydroxypinonic acid, based on the m/z 199 \rightarrow m/z 182 (loss of OH) \rightarrow m/z 155 (loss of CO_2) product ion MS/MS spectrum. The weak shoulder peak in the m/z 199 EIC likely corresponds to an isobaric compound of hydroxypinonic acid due to the presence of different product ions upon collision. The m/z 231 EIC contains five peaks. Of these, the dominant peak (RT 4.12 min) is assigned to diaterpenylic acid acetate based on its fragmentation pattern in the MS/MS spectrum: the two major ions m/z 171 and m/z 153 result from the neutral loss of CH_3COOH and H_2O molecules, respectively. The ion at m/z 247, which has been observed previously (17), is assigned to a molecular formula $\text{C}_{10}\text{H}_{16}\text{O}_5\text{S}$. The MS/MS spectrum of the parent ion at m/z 247 reveals a major product peak at m/z 97 (HSO_4^-), suggesting it contains a sulfate ester structure.

A number of dimers were observed in the mass range between m/z 300 and m/z 400. Accurate mass measurement suggests they are the extremely low volatility organic compounds (ELVOC) with molecular formula $C_{14-19}H_{24-28}O_{6-9}$. Of these, covalent dimers of the ester type, i.e., pinyl-diaterebyl ester, pinyl-diaterpenyl ester, and pinonyl-pinyl ester, have been proposed for m/z 343 (RT 5.45 min), 357, and 367, respectively (8, 9, 12-15). As shown in *SI Appendix, Figure S2 (J3–L3)*, the MS/MS spectra of these ions are in good agreement with previously published results: the collision-induced dissociation of m/z 343 (RT 5.45 min) results in m/z 157 and m/z 185; the collision-induced dissociation of m/z 357 results in m/z 185 and m/z 171; and the collision-induced dissociation of m/z 367 results in m/z 199 and m/z 185. These product ions are produced via the scission of the C–O bond in the ester structure or the C–O bond between the secondary/tertiary carbon and the alcoholic oxygen; see the fragmentation pattern sketched in *SI Appendix, Figure S3*. Further fragmentation of m/z 185 produces the m/z 141 product ion by the loss of CO_2 , which is comparable to that observed for the deprotonated pinic acid $[M-H]^-$. Similarly, further fragmentation of m/z 171 produces the m/z 127 product ion, which is comparable to that observed for the deprotonated diaterpenylic acid $[M-H]^-$. It is worth noting that there are four major peaks in the m/z 343 EIC in *SI Appendix, Figure S2 (I)*. The first peak (RT 3.96) has been attributed to a non-covalent dimer of terpenylic acid, which is produced in the electrospray process (9). The second peak (RT 5.05) is most likely an ester of terpenylic acid and diaterpenylic acid: collision-induced dissociation of this ion results in the formation of m/z 213, m/z 187, m/z 171, and m/z 127 ions, see *SI Appendix, Figure S3* for the fragmentation mechanism. The third peak (RT 5.32) co-elutes with the m/z 357 ion, indicating that this peak might be formed in the electrospray process (loss of CH_2) other than representing an actual product from the reaction of α -pinene with ozone.

In addition to the dimers (m/z 343, m/z 357, and m/z 367) that have been previously reported, a number of ions with mass to charge ratio of 300 – 400 (u) are newly identified here, including m/z 271 (RT 6.45 min), m/z 299 (RT 5.78 min), m/z 309 (RT 5.70 min), m/z 311 (RT 5.80 min), m/z 313 (RT 6.08 min), m/z 325 (RT 6.01 min), m/z 337 (RT 6.19 min), m/z 355 (RT 5.62 min), m/z 375 (RT 5.90 min), and m/z 399 (RT 5.88 min). They are assigned to molecular formulas of $C_{14}H_{24}O_5$, $C_{15}H_{24}O_6$, $C_{17}H_{26}O_5$, $C_{16}H_{24}O_6$,

$C_{16}H_{26}O_6$, $C_{17}H_{26}O_6$, $C_{18}H_{26}O_6$, $C_{18}H_{28}O_7$, $C_{17}H_{28}O_9$, and $C_{19}H_{28}O_9$, respectively, with estimated errors less than ± 10 ppm, as shown in *SI Appendix, Table S2*. Close inspection of their MS/MS spectra reveals that two ions, m/z 185 and m/z 171, are the major fragments produced upon collision-induced dissociation of the parent ions, see *SI Appendix, Figure S3 (M3 – V3)*. Further, the m/z 185 \rightarrow m/z 167 (loss of H_2O) \rightarrow m/z 141 (loss of CO_2) and m/z 171 \rightarrow m/z 127 (loss of CO_2) fragmentation patterns, which are typical for dicarboxylic acid monoanions, are commonly observed across all ions. This indicates that pinic acid and diaterpenylic acid, or their isobaric isomers, are important monomeric building blocks for these dimers.

S3.2 Quantification

S3.2.1 Particle-Phase Components Mass Concentration Retrieval

Chamber generated α -pinene SOA was collected by PILS, which operates with a duty cycle of 5 min, and then analyzed off-line by UPLC/ESI-Q-ToFMS in the negative mode. For each experiment with approximately 6 h duration (*SI Appendix, Table S1*), a total of 72 liquid samples were collected in order to capture the dynamics of individual particle-phase components during the early stage of particle growth and SOA aging. It is worth noting that the liquid column separation prior to the electrospray ionization process precludes ionization suppression caused by potential interfering compounds mixed with the analyte, thus facilitating molecular-level quantification of particle-phase components. For any given species i , its particle-phase mass concentration, $C_{p,i}$ ($\mu\text{g m}^{-3}$), in the chamber is given by:

$$C_{p,i} = \frac{1000 \cdot R_i \cdot Q_1 \cdot DF \cdot \rho_1}{IE_i \cdot Q_g \cdot CE_{\text{PILS}}} \quad (\text{S1})$$

where 1000 is the unit conversion factor, R_i is the ESI-Q-ToFMS response towards the ion ($[M - H]_i^-$) produced via deprotonation of compound i in the negative mode, Q_1 is the liquid sampling flow rate (1.5 mL min^{-1}), DF is the dilution factor that accounts for the water vapor condensation on the PILS impactor wall, ρ_1 is the density of collected liquid, which is assumed to be the density of the washing flow (0.893 g cm^{-3}), which is composed of 50% Milli-Q water and 50% isopropyl alcohol, Q_g is the gas sampling flow

rate (12.5 L min⁻¹), IE_i is the electrospray ionization efficiency (sensitivity) of compound i , and CE_{PILS} is the collection efficiency of PILS for α -pinene+O₃ derived SOA. Here a collection efficiency of 0.8–0.9 is used based on a linear relationship between CE_{PILS} and the particulate average O:C ratio developed in our recent studies (18).

S3.2.2 Electrospray Ionization Efficiency Estimation

The ESI process proceeds via the ion evaporation mechanism in the case of low molecular weight compounds (19, 20). The electrospray conditions and molecular structures of analytes govern the ionization efficiency. Since the ESI-MS operation parameters are controlled consistently in the present study, the ionization efficiency of individual products identified here is expected to depend strongly on their physicochemical properties, such as molecule size, pK_a value, hydrophobicity, surface activity, etc. (21). The ionization efficiency of pinonic acid is obtained directly from the counts/concentration calibration curve of commercially available *cis*-pinonic acid standard (Sigma-Aldrich, 98% purity). The ionization efficiency of other products identified in *SI Appendix, Table S2* is estimated based on a linear model developed by Krueve et al. (22):

$$\log RIE_i = (1.04 \pm 0.34) + (2.23 \pm 0.34) \cdot \alpha_i + (-0.51 \pm 0.04) \cdot WAPS_i \cdot 10^5 \quad (S2)$$

where RIE_i is the relative ionization efficiency of compound i relative to benzoic acid via deprotonation in the negative mode, α_i is the degree of ionization for compound i , which is calculated based on its pK_a and the pH of the aqueous phase, and $WAPS_i$ (weighted average positive sigma) is a parameter defined as the weighted mean of positive sigma (σ) values divided by the ion surface area (23):

$$WAPS = \frac{\int_{\sigma=0}^{\infty} \sigma \cdot p(\sigma) \cdot d\sigma}{A \int_{\sigma=0}^{\infty} p(\sigma) \cdot d\sigma} \quad (S3)$$

where σ is the polarization charge density on the ion surface, $p(\sigma)$ is the probability function of σ (sigma profile), and A is the surface area of the anion.

COnductor-like Screening MOdel for Real Solvents (COSMO-RS) method (24) implemented into the Amsterdam Density Functional (ADF 2014.07) molecular modeling suite (25) was used for calculating pK_a of individual compounds dissolved in

water/acetonitrile mixture, as well as generating the sigma profiles needed for calculating the *WAPS* parameter. First, 18 molecules were chosen from *SI Appendix, Table S2* and the proper structure and connectivity of each molecule was drawn in three dimensions in the ADF tool. Different conformations were considered and the conformers with lowest energy were adopted. Next, the molecular geometries were optimized at the TZP level with the Becke-Perdew (BP) Generalized Gradient Approximation (GGA) density functional. By doing so, the ideal-gas phase-equilibrium geometry for each molecule can be obtained. Second, a COSMO calculation was carried out on all species using the ADF input files to calculate the screening charges mapped on the cavity surface surrounding the molecule in the condensed phase. Here, hydrogen bonding was taken into account, which is particularly necessary for large molecules so that the monoanion adopts a ‘coiled’ conformation placing the ionized carboxyl group with a labile hydrogen atom in close proximity. It is worth noting that the atomic radii for the four elements, i.e., carbon, hydrogen, oxygen, and sulfur, have been included and optimized in the COSMO-RS approach. Finally, using the calculated charge density distribution, we can calculate the charge delocalization in the species, as represented by the parameter *WAPS*.

The aqueous pK_a of each compound, denoted as ${}^w pK_a$, was calculated based on its free energy of dissociation in water (ΔG_{diss}^*). The cluster-continuum approach in the COSMO-RS model was employed to compute the ΔG_{diss}^* values. It has been recommended that the cluster-continuum approach can predict the aqueous pK_a for strong to moderately weak acids with reasonable accuracy (26). Molecules that have two or more equivalent sites for deprotonation (e.g., dicarboxylic acids) were not taken into account, so the predicted aqueous pK_a values are only for the dissociation of the first proton (pK_{a1}). Here it is not necessary to predict pK_{a2} since di-anions were not observed during the electrospray ionization of dicarboxylic acids. It is important to note that when an analyte elutes from the LC column, the solvent composition for this particular analyte depends on the eluent program: the volume fraction of acetonitrile in the water/acetonitrile solvent mixture increases linearly from ~20% to ~50% from retention time 3.6 min to retention time 7.2 min. To account for the explicit solvent molecules, we applied a linear model developed by Espinosa et al. (27). In this way, the pK_a value of an

analyte in the water/acetonitrile mixture (${}^s\text{p}K_a$) can be accurately predicted from its corresponding $\text{p}K_a$ value in water (${}^w\text{p}K_a$), with standard deviation less than 0.3 $\text{p}K_a$ unit:

$${}^s\text{p}K_a = a_s \times {}^w\text{p}K_a + b_s \quad (\text{S4})$$

where a_s is related to difference between specific solvation interactions, which depend on the solvent and family of compounds, and b_s is related to the difference in basicities, dielectric constants, and specific solvation interactions of the solute between the organic solvent, which is acetonitrile here, and water. Specific values used for a_s and b_s in this study are referred to Table 2 in the original paper.

The pH of the LC solvent, i.e., acetonitrile/water mixture, was directly measured using a digital pH meter (VWR Scientific Model 8010), with its electrode calibrated with standard aqueous buffers. The pH obtained herein is denoted as ${}^w\text{pH}$, namely, pH measured in acetonitrile/water mixture and referred to water as standard state. The ‘ δ ’ factor is applied to convert ${}^w\text{pH}$ to ${}^s\text{pH}$, i.e., pH measured in acetonitrile/water mixture and referred to the same acetonitrile/water mixture as standard state, with standard deviation less than 0.02 pH unit (28):

$${}^s\text{pH} = {}^w\text{pH} - \delta \quad (\text{S5})$$

Here the ‘ δ ’ term represents the primary medium effect and the difference between the liquid-junction potentials of the electrode system in solvent mixture and water. Specific values used for δ in this study are referred to Equation (10) in the original paper.

Finally, the degree of ionization for each analyte (α) in the LC mobile phase (v/v % acetonitrile/water) can be calculated given the estimated ${}^s\text{p}K_a$ value for each compound and the ${}^s\text{pH}$ of the mobile phase:

$$\alpha = \frac{10^{-{}^s\text{p}K_a}}{10^{-{}^s\text{p}K_a} + 10^{-{}^s\text{pH}}} \quad (\text{S6})$$

SI Appendix, Figure S4 shows the COSMO-RS computed sigma profiles for 6 negative ions (m/z 171, 183, 231, 247, 357, and 367) identified in this study. The sigma profile presents the probability distribution of a molecular surface segment that has a specific charge density (29). For each ion, its sigma profile contains 90 segments, 0.0089

$e/\text{\AA}^2$ wide, in the range of $-0.04 e/\text{\AA}^2$ to $0.04 e/\text{\AA}^2$. Given the sigma profiles, we can calculate the weighted average positive sigma (*WAPS*) via Equation (S3). The smaller the *WAPS* value, the more delocalized the charge in the anion. The effect of charge delocalization on the electrospray ionization efficiency can be explained by the charge to charge repulsion occurring on the ESI droplet (22). The more delocalized the charge in the anion, the more charge to charge repulsion occurs between ions, the more likely ions evaporates from the ESI droplet, and as a result, the higher ionization efficiency of the parent molecule. It can be seen that the calculated relative ionization efficiency towards *cis*-pinonic acid standard (*RIE*) strongly depends on the *WAPS* parameter. For example, the *RIE* of *m/z* 367 is ~ 7 times higher than that for *cis*-pinonic acid, given the corresponding *WAPS* values of 2.58×10^{-5} and 4.25×10^{-5} , respectively. The effect of the pK_a parameter on the ionization efficiency lies in the abundance of ionizable components in the droplets. A straightforward illustration would be that strong acids tend to completely dissociate in the aqueous solution and present as the conjugate base ($\text{HA} \rightarrow \text{H}^+ + \text{A}^-$). As a result, compounds with relatively low pK_a values tend to give a high response in the ESI negative mode. For example, the *RIE* of *m/z* 247, which represents a sulfate ester, is approximately two orders magnitude higher than that for *cis*-pinonic acid.

S3.2.3 Uncertainty Analysis

Uncertainties in the PILS particle sampling technique arise mainly from variation of the collected liquid volume due to the existence of air bubbles. We have estimated in the PILS+UPLC/ESI-Q-ToFMS methodology study that this uncertainty is less than $\pm 11\%$ (16). Next, we need to evaluate the uncertainties that arise from the electrospray ionization efficiency calculation. Since we have used a linear model that is developed based on optimal fitting of the predicted ionization efficiency to the corresponding measurements, we focus on the resulting uncertainties by employing this linear model to predict the *RIE* of the identified species. While we acknowledge uncertainties from the prediction of thermodynamic properties of molecules using the COSMO-RS software, it is important to note that these uncertainties have been incorporated in the linear model. *SI Appendix, Table S2* gives the predicted *RIE* of each product identified from the α -pinene SOA system relative to that of the *cis*-pinonic acid standard as well as the corresponding

uncertainties. It can be seen that the parameter, *WAPS*, contributes to most of the simulation uncertainties, whereas uncertainty resulting from the pK_a parameter is insignificant. This is due to the LC conditions employed in this study: most products are not dissociated at pH of 2–3 and are present in molecular form in the mobile phase prior to ESI.

S4. Vapor-Particle Dynamics Model

A modified version of the Vapor-Particle Dynamics Model was used to simulate the proposed mechanism for the $C_{17}H_{26}O_6$ ester dimer formation during the ozonolysis of α -pinene. Details of the model can be found in the original paper (30), and only an overview and the additional modifications are presented here. The model simulates gas/condensed-phase reactions, condensation/evaporation of gas-phase compounds to produce organic aerosol, particle-wall deposition, and vapor-wall interactions in a well-mixed laboratory chamber. A moving-bin version of the model is used to represent the single distribution of the chamber aerosol, and coagulation is neglected.

The gas- and particle-phase reactions simulated are given in *SI Appendix, Table S4*. These reactions are not intended to represent the full mechanism for the ozonolysis of α -pinene but rather involve species only contributing to the formation of the $C_{17}H_{26}O_6$ ester dimer. The particle-phase decomposition of the diacyl peroxide to form the ester is added to the mechanism, which did not originally include particle-phase reactions. Reactions G01 through G10 are taken from MCMv3.2 (<http://mcm.leeds.ac.uk/MCM>). The rate constants for G07 and G10 were changed to $5 \times 10^{-12} \text{ cm}^3 \text{ molec}^{-1} \text{ s}^{-1}$ based on the mean of primary, secondary, and tertiary RO_2 reaction rate constants (31). The rate constants and molar product yields for reactions G11, P01, and P02 were optimized in order to match the observed particle-phase concentration of the $C_{17}H_{26}O_6$ ester dimer. Because the model does not simulate inorganic chemistry or the full α -pinene ozonolysis mechanism, O_3 , OH, HO_2 , and RO_2 concentrations are needed as inputs (no OH scavenger was used during the experiment, and thus the ozonolysis of α -pinene generates OH as a coproduct). The O_3 concentration was measured experimentally. This experimental curve was fit to a fourth-order Gaussian function and used in the model to determine the O_3 concentration at each moment in time. OH, HO_2 , and RO_2 concentrations were not measured

experimentally. Therefore, concentrations for these species were predicted using the Generator for Explicit Chemistry and Kinetics of Organics in the Atmosphere (GECKO-A) (32) using the corresponding experimental conditions (154 ppb α -pinene, 200 ppb O_3 , zero NO_x , 298 K, and $< 5\%$ RH) as the input. The OH, HO_2 , and RO_2 curves generated by GECKO-A were also fit to fourth-order Gaussian functions which were then implemented in the model. For simulations with initial mixing ratios of 10 ppb α -pinene + 20 ppb O_3 , concentrations of reactants and free radicals were predicted by GECKO-A as well.

The two stable gas-phase species, pinic acid ($C_9H_{14}O_4$) and the diacyl peroxide ($C_{18}H_{26}O_8$), condense onto both seed particles and the chamber walls. The rate of condensation onto particles is controlled by the vapor-particle accommodation coefficient. The optimal vapor-particle accommodation coefficient was determined separately for each of the two compounds in order to match the observed particle-phase concentration. An accommodation coefficient of 0.01 was determined for pinic acid, and an accommodation coefficient of 0.1 was determined for the diacyl peroxide. The vapor pressures of pinic acid and the diacyl peroxide are listed in *SI Appendix, Table S4*. The organic aerosol concentration was measured experimentally using the SMPS. The 2-Product model was fit to the observed ΔM_o (the total organic aerosol mass produced) vs. ΔHC (the mass of hydrocarbon reacted) curve and was then used to predict the SOA yield at low organic mass loadings.

Condensation onto the chamber walls is treated as an equilibration process, characterized by an effective organic concentration in the walls (C_w), which is set to 10 mg m^{-3} (33). The vapor wall loss rates for the two condensable species, pinic acid and the diacyl peroxide, were predicted using the empirical expression derived by Zhang et al. (34) relating the vapor-wall accommodation to the species vapor pressure. The predicted wall loss rates are listed in *SI Appendix, Table S4*. The initial size distribution of the inorganic seed particles is lognormal with a standard deviation of 1.5 and a number concentration determined experimentally using the SMPS. Particle wall losses were implemented using the diameter-dependent wall loss rates measured experimentally in the Caltech chamber. The quantities of pinic acid and diacyl peroxide that condensed on

particles that subsequently deposited on the chamber walls are considered lost from the simulation.

References:

1. Loza CL, et al. (2014) Secondary organic aerosol yields of 12-carbon alkanes. *Atmos Chem Phys* 14(3):1423-1439.
2. Zhang X, et al. (2014) Role of ozone in SOA formation from alkane photooxidation. *Atmos Chem Phys* 14(3):1733-1753.
3. Canagaratna, et al. (2015) Elemental ratio measurements of organic compounds using aerosol mass spectrometry: characterization, improved calibration, and implications. *Atmos. Chem. Phys.* 15, 253-272, 2015.
4. Chhabra PS, Flagan RC, Seinfeld JH (2010) Elemental analysis of chamber organic aerosol using an aerodyne high-resolution aerosol mass spectrometer. *Atmos Chem Phys* 10(9):4111-4131.
5. Jenkin ME, Shallcross DE, Harvey JN (2000) Development and application of a possible mechanism for the generation of cis-pinic acid from the ozonolysis of alpha- and beta-pinene. *Atmos Environ* 34(18):2837-2850.
6. Jaoui M, Kamens RM (2001) Mass balance of gaseous and particulate products analysis from alpha-pinene/NO_x/air in the presence of natural sunlight. *J Geophys Res-Atmos* 106(D12):12541-12558.
7. Ma Y, Russell AT, Marston G (2008) Mechanisms for the formation of secondary organic aerosol components from the gas-phase ozonolysis of alpha-pinene. *Phys Chem Chem Phys* 10(29):4294-4312.
8. Muller L, Reinnig MC, Warnke J, Hoffmann T (2008) Unambiguous identification of esters as oligomers in secondary organic aerosol formed from cyclohexene and cyclohexene/alpha-pinene ozonolysis. *Atmos Chem Phys* 8(5):1423-1433.
9. Claeys M, et al. (2009) Terpenylic acid and related compounds from the oxidation of alpha-pinene: implications for new particle formation and growth above forests. *Environ Sci Technol* 43(18):6976-6982.
10. Camredon M, et al. (2010) Distribution of gaseous and particulate organic composition during dark alpha-pinene ozonolysis. *Atmos Chem Phys* 10(6):2893-2917.
11. Gao YQ, Hall WA, Johnston MV (2010) Molecular composition of monoterpene secondary organic aerosol at low mass loading. *Environ Sci Technol* 44(20):7897-7902.

12. Yasmeen F, et al. (2010) Terpenylic acid and related compounds: precursors for dimers in secondary organic aerosol from the ozonolysis of alpha- and beta-pinene. *Atmos Chem Phys* 10(19):9383-9392.
13. Kristensen K, et al. (2013) Formation and occurrence of dimer esters of pinene oxidation products in atmospheric aerosols. *Atmos Chem Phys* 13(7):3763-3776.
14. Kristensen K, et al. (2014) Dimers in alpha-pinene secondary organic aerosol: effect of hydroxyl radical, ozone, relative humidity and aerosol acidity. *Atmos Chem Phys* 14(8):4201-4218.
15. Witkowski B, Gierczak T (2014) Early stage composition of SOA produced by alpha-pinene/ozone reaction: alpha-acyloxyhydroperoxy aldehydes and acidic dimers. *Atmos Environ* 95:59-70.
16. Bandu ML, Watkins KR, Bretthauer ML, Moore CA, Desaire H (2004) Prediction of MS/MS data. 1. a focus on pharmaceuticals containing carboxylic acids. *Anal Chem* 76(6):1746-1753.
17. Liggio J, Li SM (2006) Reactive uptake of pinonaldehyde on acidic aerosols. *J Geophys Res-Atmos* 111(D24).
18. Zhang X, et al. (2015) Time-resolved molecular characterization of organic aerosols by PILS + UPLC/ESI-Q-TOFMS. *Atmos Environ* 10.1016/j.atmosenv.2015.08.049.
19. Enke CG (1997) A predictive model for matrix and analyte effects in electrospray ionization of singly-charged ionic analytes. *Anal Chem* 69(23):4885-4893.
20. Kebarle P (2000) Gas phase ion thermochemistry based on ion-equilibria From the ionosphere to the reactive centers of enzymes. *Int J Mass Spectrom* 200(1-3):313-330.
21. Oss M, Krueve A, Herodes K, Leito I (2010) Electrospray ionization efficiency scale of organic compounds. *Anal Chem* 82(7):2865-2872.
22. Krueve A, Kaupmees K, Liigand J, Leito I (2014) Negative electrospray ionization via deprotonation: predicting the ionization efficiency. *Anal Chem* 86(10):4822-4830.
23. Kaupmees K, Kaljurand I, Leito I (2010) Influence of water content on the acidities in acetonitrile. quantifying charge delocalization in anions. *J Phys Chem A* 114(43):11788-11793.
24. Klamt A (1995) Conductor-like screening model for real solvents - a new approach to the quantitative calculation of solvation phenomena. *J Phys Chem-US* 99(7):2224-2235.
25. Pye CC, Ziegler T, van Lenthe E, Louwen JN (2009) An implementation of the conductor-like screening model of solvation within the Amsterdam density functional package - Part II. COSMO for real solvents. *Can J Chem* 87(7):790-797.

26. Eckert F, Diedenhofen M, Klamt A (2010) Towards a first principles prediction of pK(a): COSMO-RS and the cluster-continuum approach. *Mol Phys* 108(3-4):229-241.
27. Espinosa S, Bosch E, Roses M (2002) Retention of ionizable compounds in high-performance liquid chromatography - 14. acid-base pK values in acetonitrile-water mobile phases. *J Chromatogr A* 964(1-2):55-66.
28. Espinosa S, Bosch E, Roses M (2000) Retention of ionizable compounds on HPLC. 5. pH scales and the retention of acids and bases with acetonitrile-water mobile phases. *Anal Chem* 72(21):5193-5200.
29. Mullins E, et al. (2006) Sigma-profile database for using COSMO-based thermodynamic methods. *Ind Eng Chem Res* 45(12):4389-4415.
30. McVay RC, Cappa CD, Seinfeld JH (2014) Vapor-wall deposition in chambers: theoretical considerations. *Environ Sci Technol* 48(17):10251-10258.
31. Orlando JJ, Tyndall GS (2012) Laboratory studies of organic peroxy radical chemistry: an overview with emphasis on recent issues of atmospheric significance. *Chem Soc Rev* 41(19):6294-6317.
32. Aumont B, Szopa S, Madronich S (2005) Modelling the evolution of organic carbon during its gas-phase tropospheric oxidation: development of an explicit model based on a self generating approach. *Atmos Chem Phys* 5:2497-2517.
33. Zhang X, et al. (2014) Influence of vapor wall loss in laboratory chambers on yields of secondary organic aerosol. *P Natl Acad Sci USA* 111(16):5802-5807.
34. Zhang X, et al. (2015) Vapor wall deposition in Teflon chambers. *Atmos Chem Phys* 15(8):4197-4214.
35. Crouse JD, Nielsen LB, Jorgensen S, Kjaergaard HG, Wennberg PO (2013) Autoxidation of organic compounds in the atmosphere. *J Phys Chem Lett* 4(20):3513-3520.
36. Rissanen MP, et al. (2014) The formation of highly oxidized multifunctional products in the ozonolysis of cyclohexene. *J Am Chem Soc* 136(44):15596-15606.

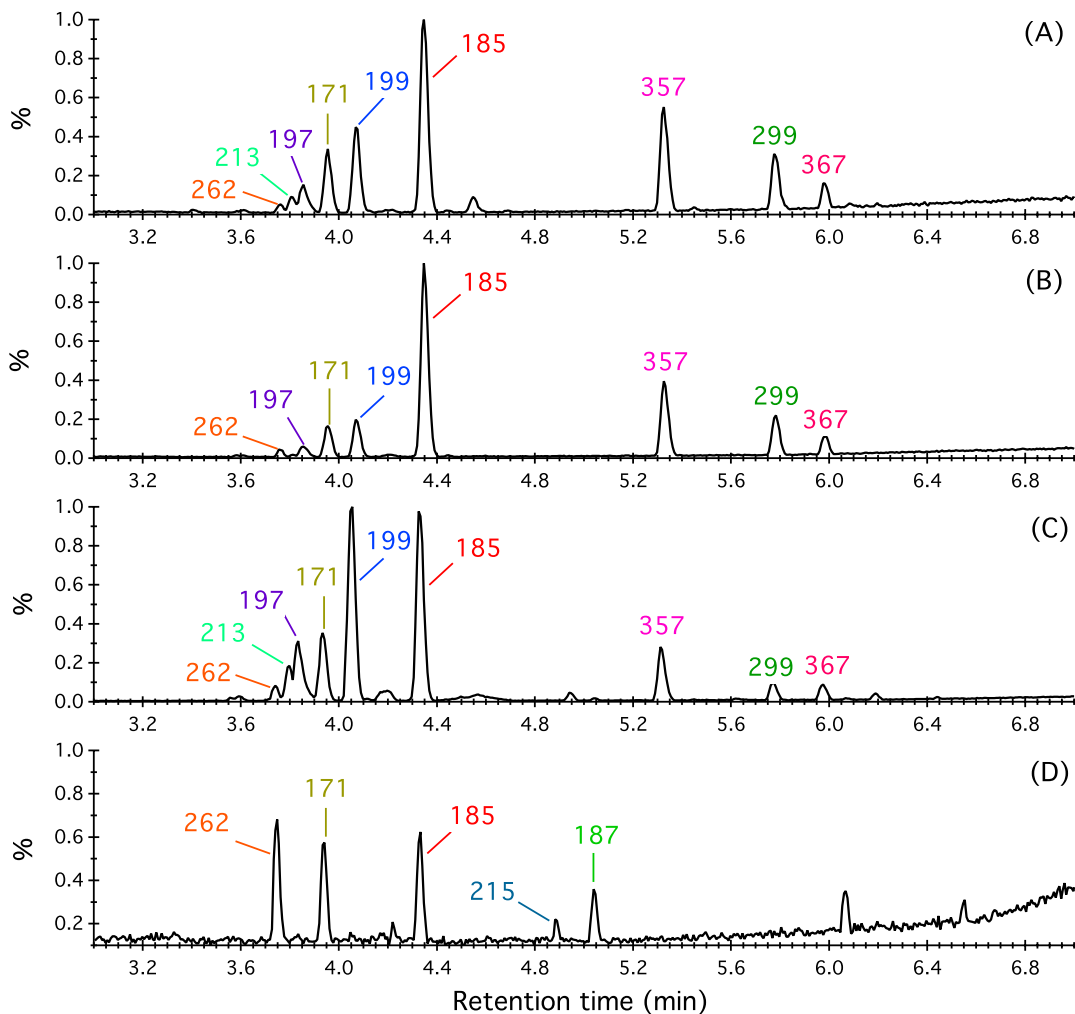
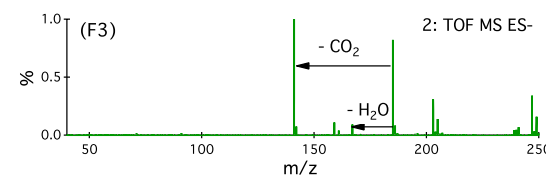
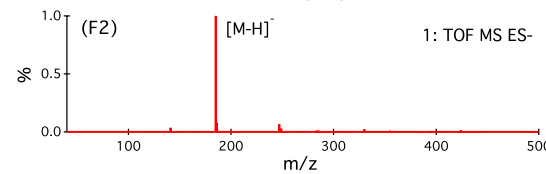
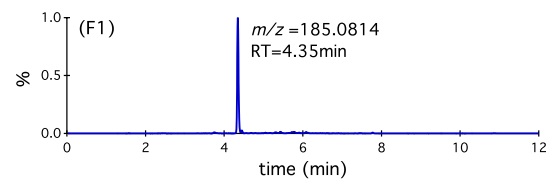
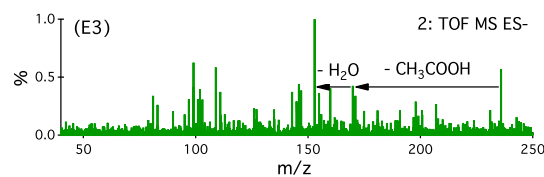
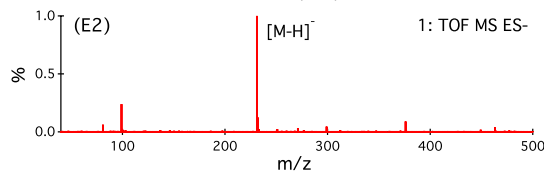
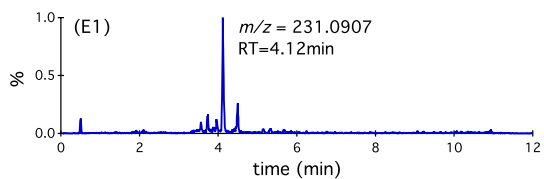
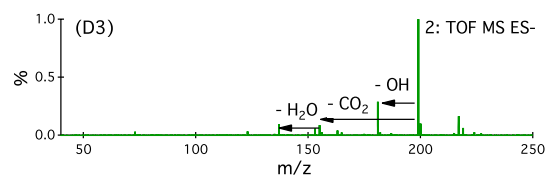
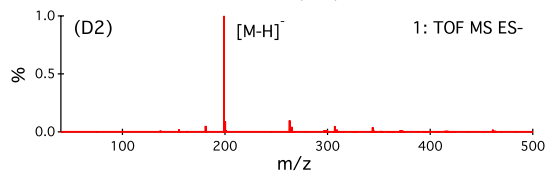
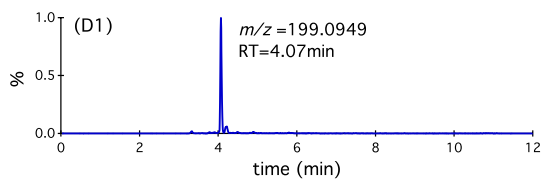
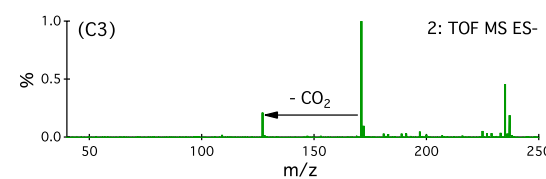
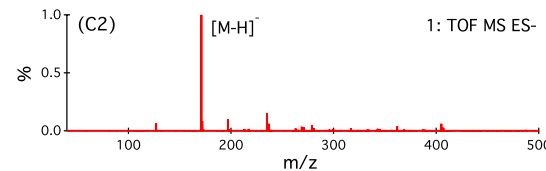
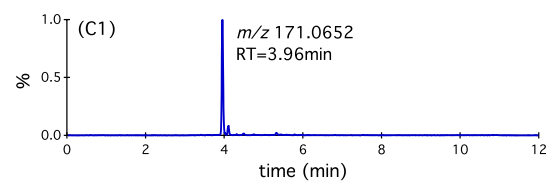
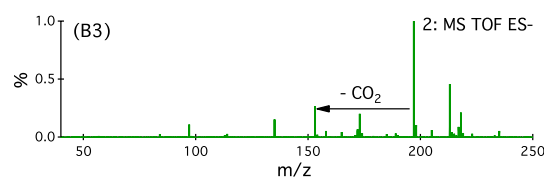
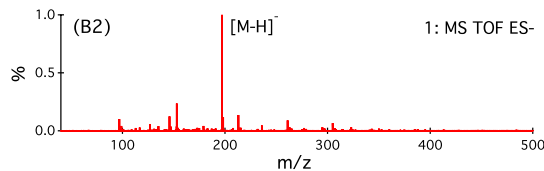
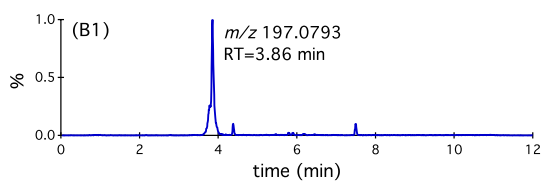
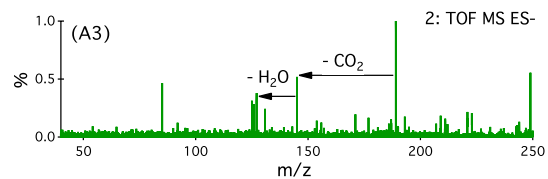
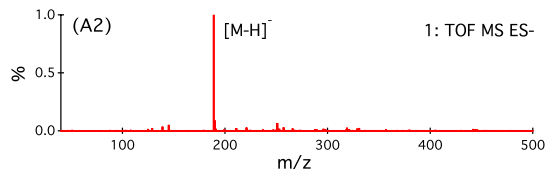
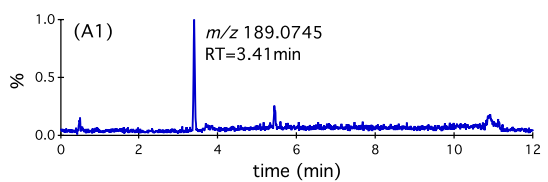
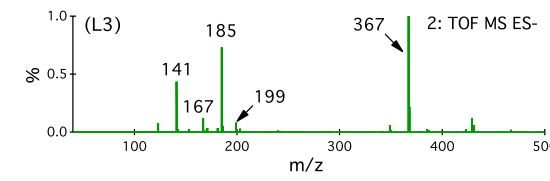
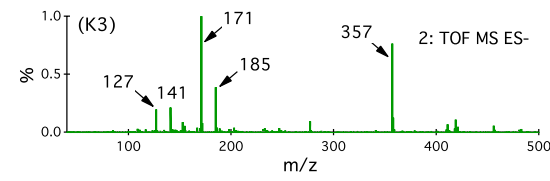
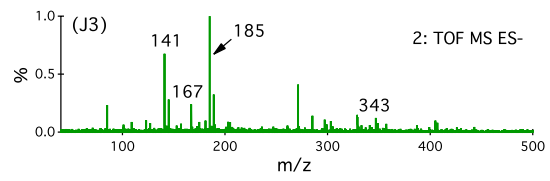
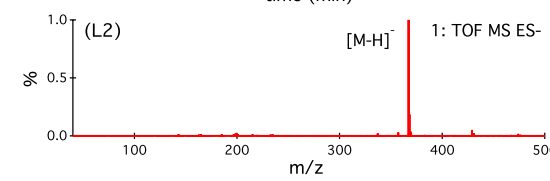
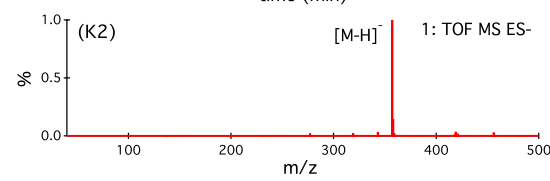
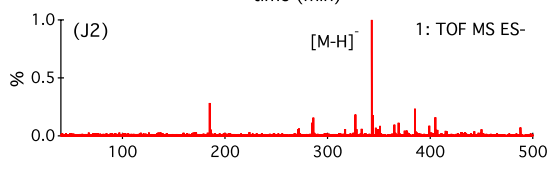
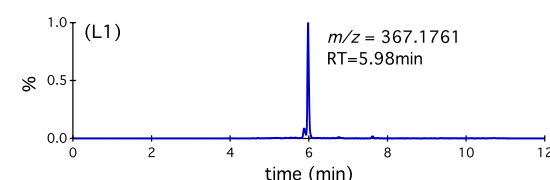
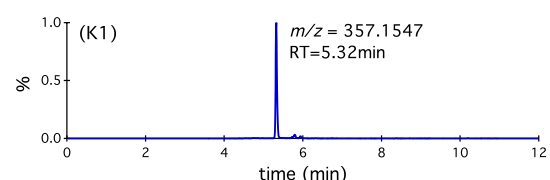
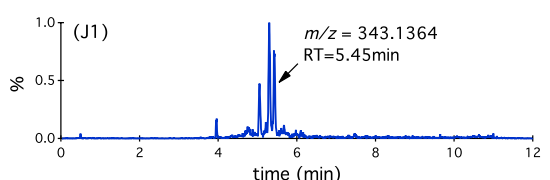
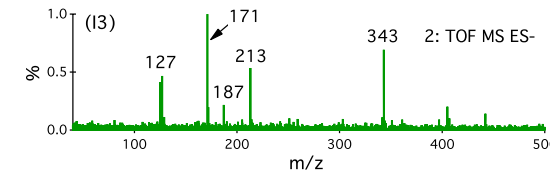
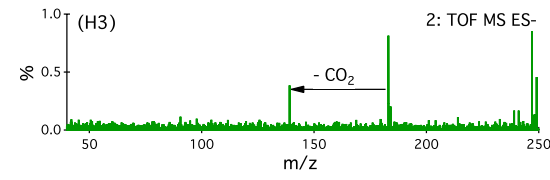
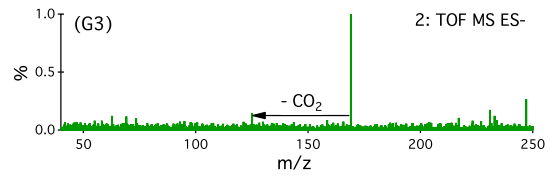
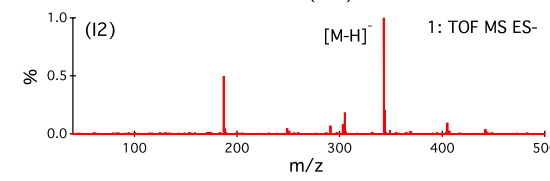
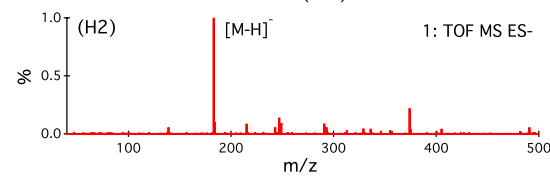
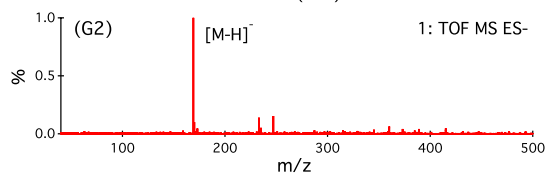
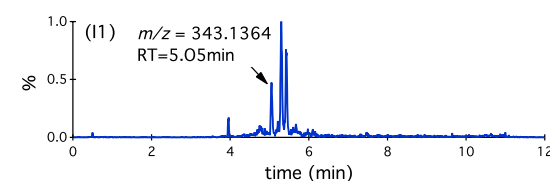
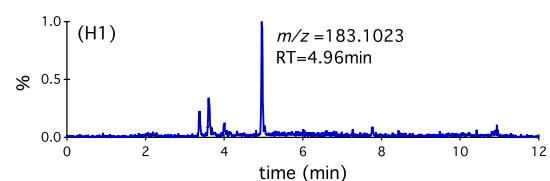
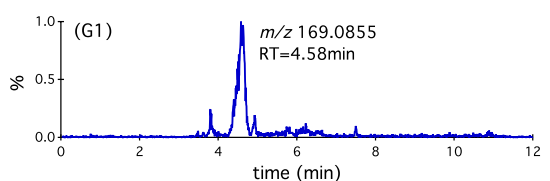
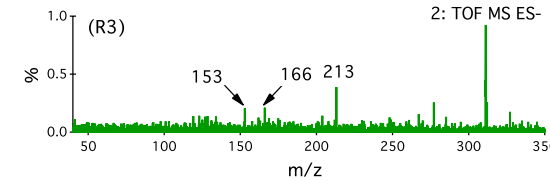
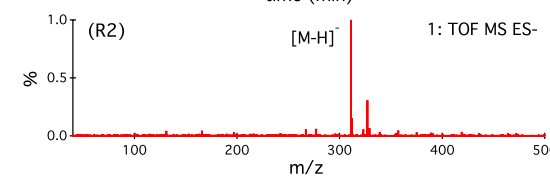
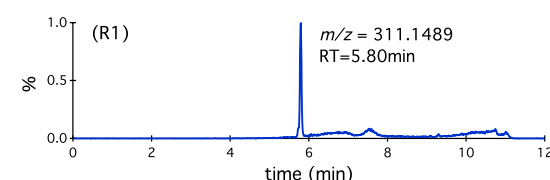
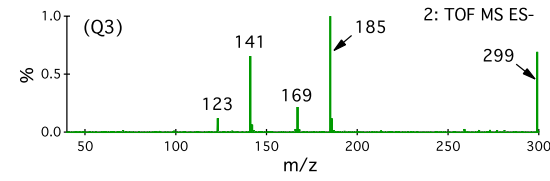
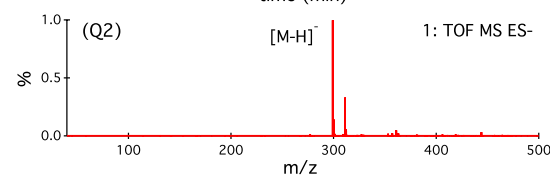
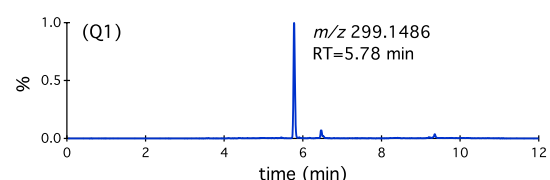
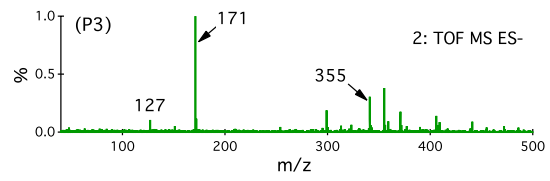
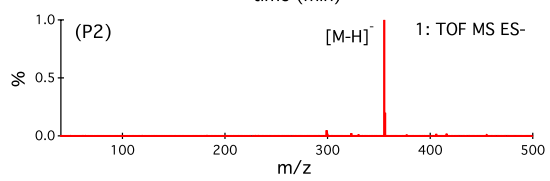
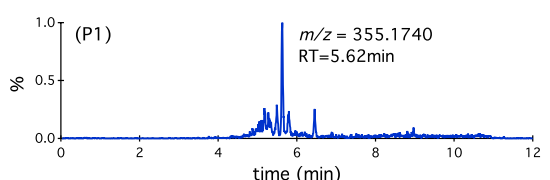
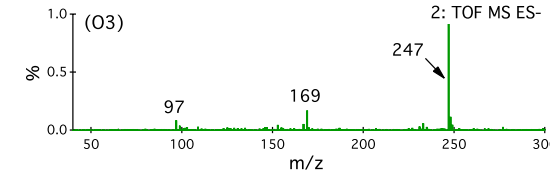
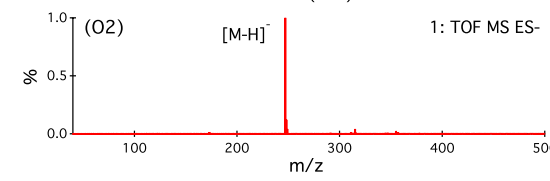
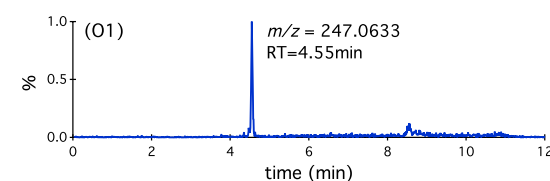
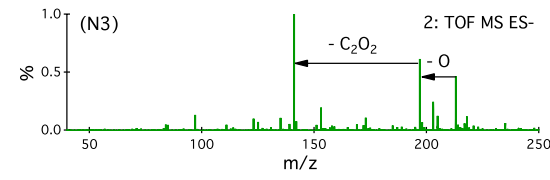
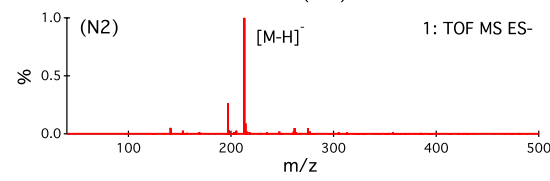
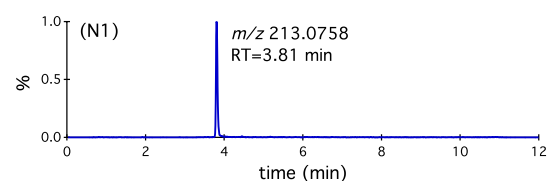
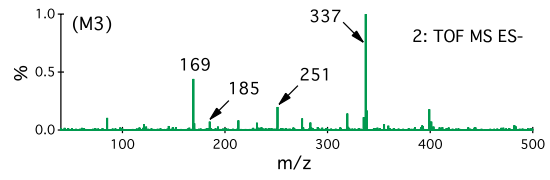
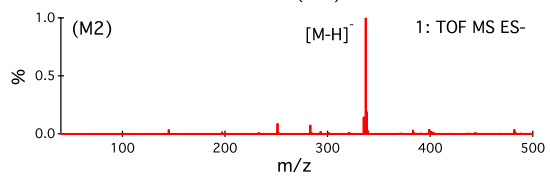
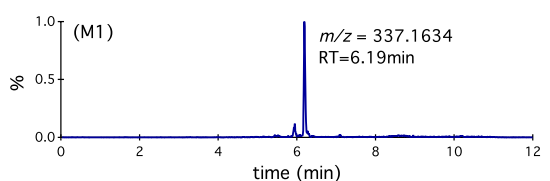


Figure S1. UPLC/(-)ESI-Q-ToFMS base peak chromatographs (BPCs) of particle-phase constituents produced from (A) dark ozonolysis of α -pinene at 298 K and 5% RH; (B) dark ozonolysis of α -pinene at 298 K and 50% RH; (C) dark ozonolysis of α -pinene at 285 K and 5% RH; and (D) OH-initiated oxidation of α -pinene at 298 K and 5% RH. The numbers listed next to each peak correspond to the respective $[M-H]^-$ ions generated in the ESI negative mode. Ions at m/z 171, 199, and 185 correspond to terpenylic acid, OH-pinonic acid, and pinic acid, respectively. These three monomers are detected in SOA from both OH-initiated and O_3 -initiated oxidation of α -pinene.







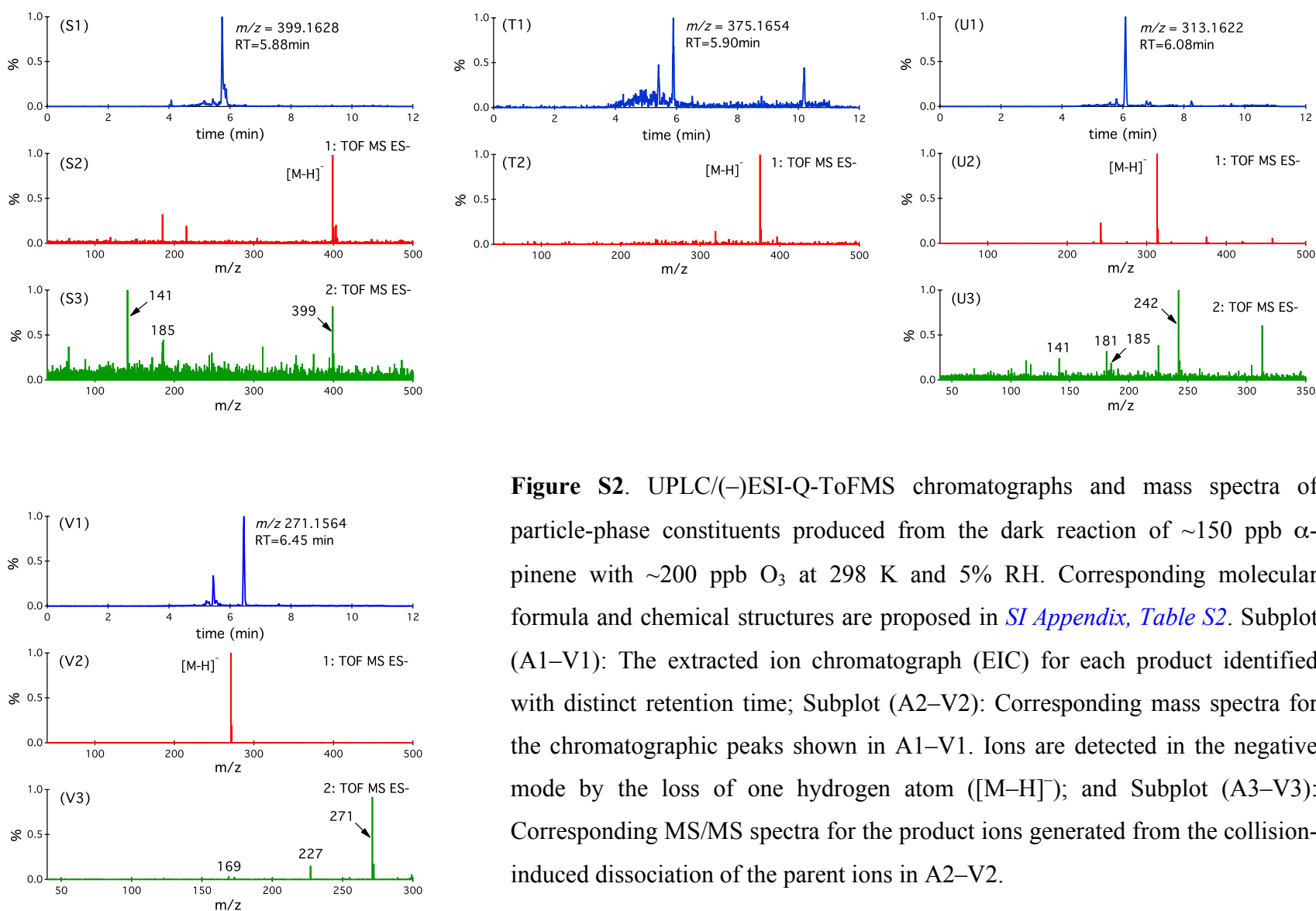


Figure S2. UPLC/(-)ESI-Q-ToFMS chromatographs and mass spectra of particle-phase constituents produced from the dark reaction of ~ 150 ppb α -pinene with ~ 200 ppb O_3 at 298 K and 5% RH. Corresponding molecular formula and chemical structures are proposed in *SI Appendix, Table S2*. Subplot (A1–V1): The extracted ion chromatograph (EIC) for each product identified with distinct retention time; Subplot (A2–V2): Corresponding mass spectra for the chromatographic peaks shown in A1–V1. Ions are detected in the negative mode by the loss of one hydrogen atom ($[M-H]^-$); and Subplot (A3–V3): Corresponding MS/MS spectra for the product ions generated from the collision-induced dissociation of the parent ions in A2–V2.

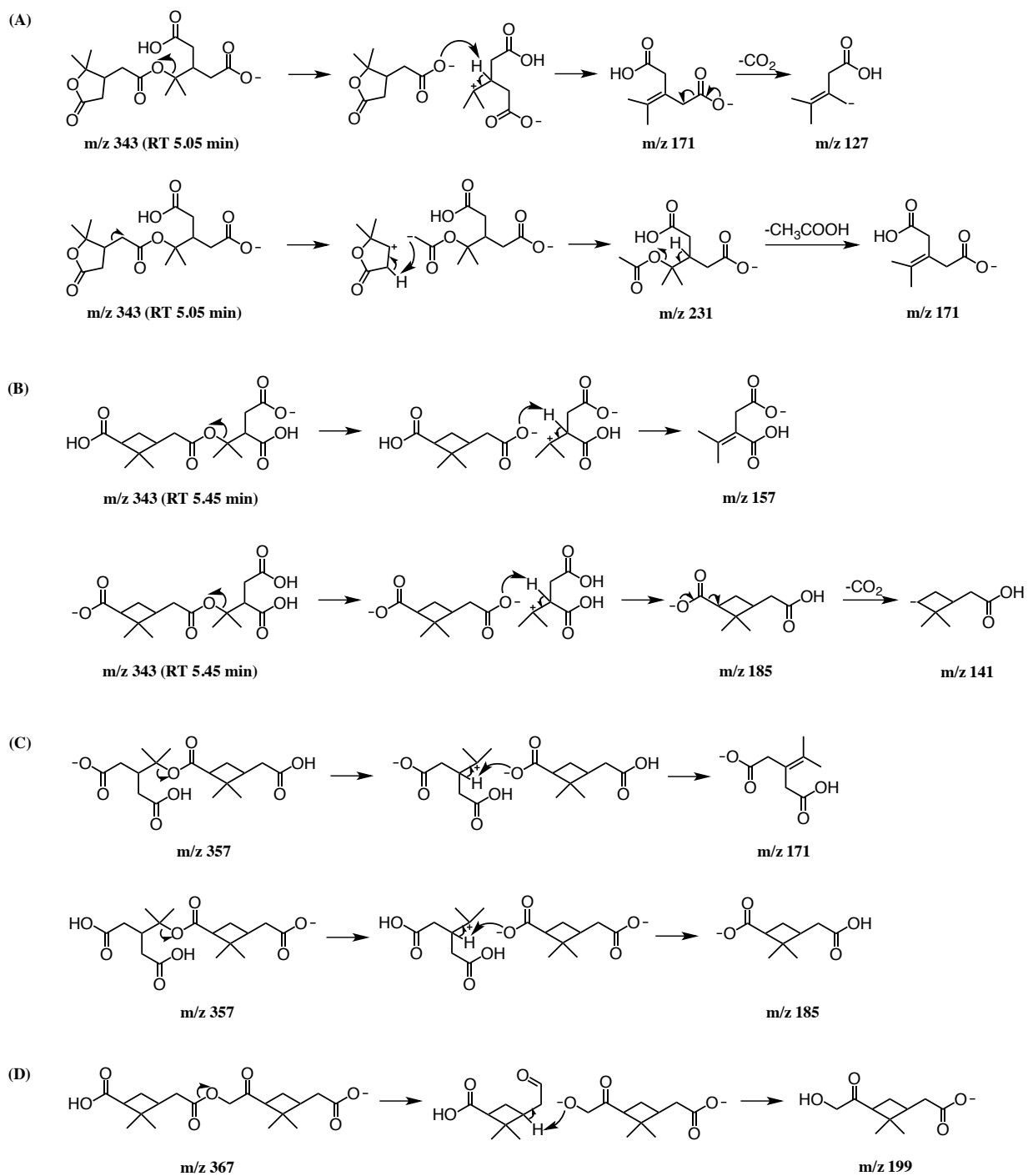


Figure S3. Fragmentation pathways of negative ions at m/z 343, m/z 357, and m/z 367 examined by collision induced dissociation (CID).

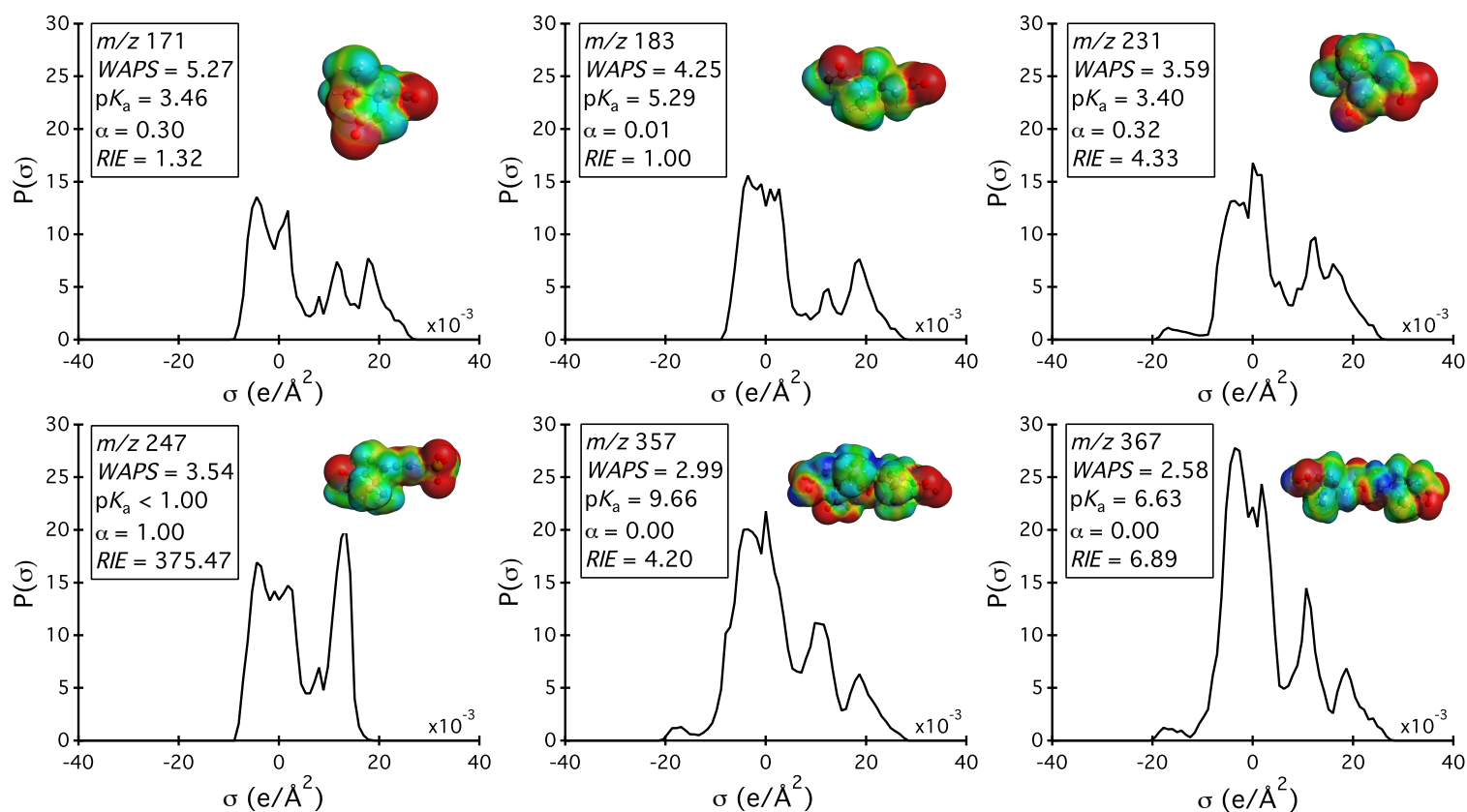


Figure S4. Sigma profiles of negative ions ($[M-H]^-$) at m/z 171, 183, 231, 247, 357, and 367. The structure of each ion is shown in the format of the COSMO charge density on a COSMO surface visualized with ADFview. Note that the red color represents positive COSMO charge density (the underlying molecular charge is negative), and the blue color represents negative COSMO charge density (the underlying molecular charge is positive). The calculated $WAPS$ ($\times 10^5$), s_pK_a , degree of ionization (α), and relative ionization efficiency (RIE_i) to pinonic acid are also shown for each ion.

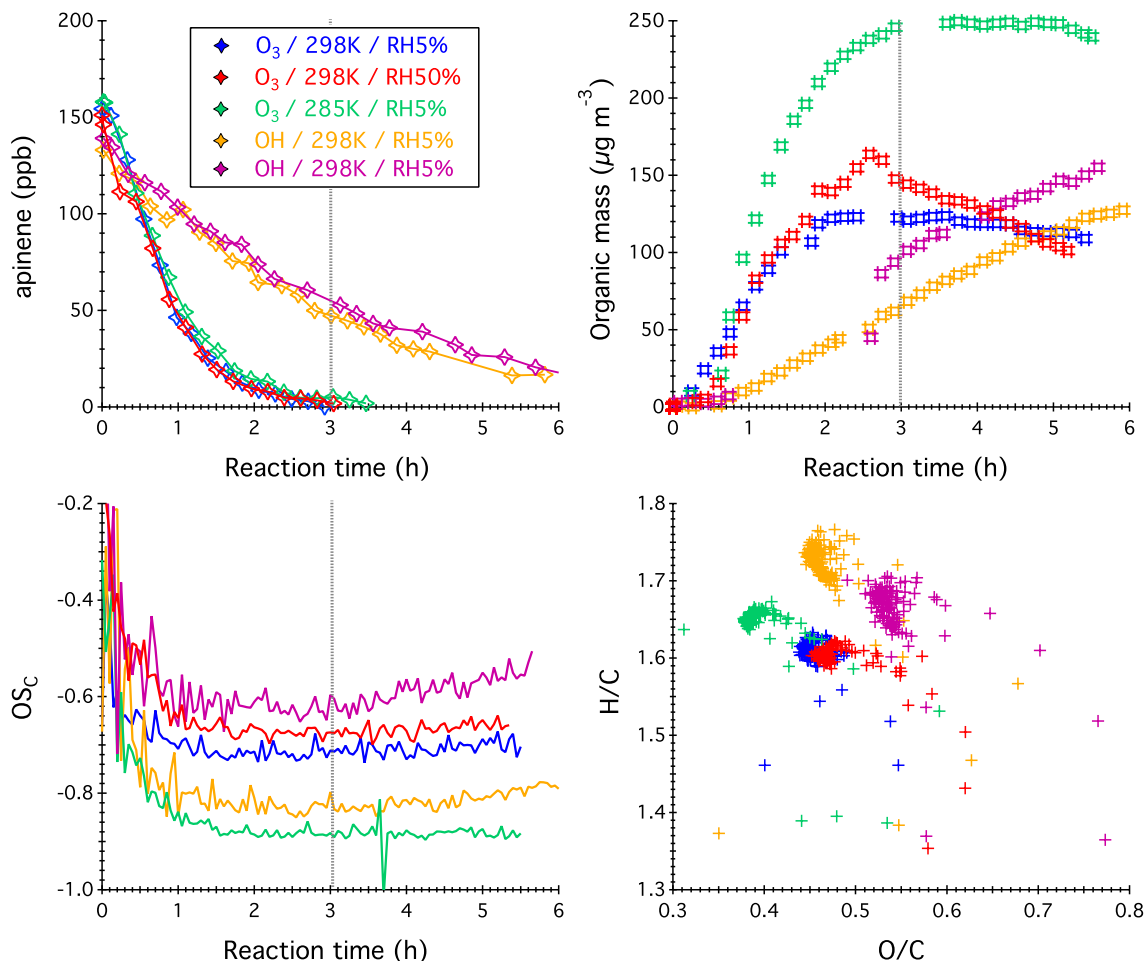


Figure S5. Organic mass concentration and molecular composition of α -pinene SOA. Experimental conditions are listed in *SI Appendix, Table S1*. The gray dashed lines denote the 5-min average time period at which the SOA chemical composition measured by PILS+UPLC/(–)ESI-Q-ToFMS is shown in [Figure 1](#) and [Figure 2](#). (A) GC-FID measured decay of α -pinene due to reaction with O_3 and OH. (B) DMA measured overall organic mass growth. Note that particle wall loss is not applied here in order to directly compare with the total mass of PILS collected suspended particle via the sum of individual compounds. (C) AMS measured average O:C and H:C ratios of α -pinene SOA in the van Krevelen diagram. (D) Progression of the derived oxidation state ($OS_C = 2 \times O/C - H/C$) of α -pinene SOA.

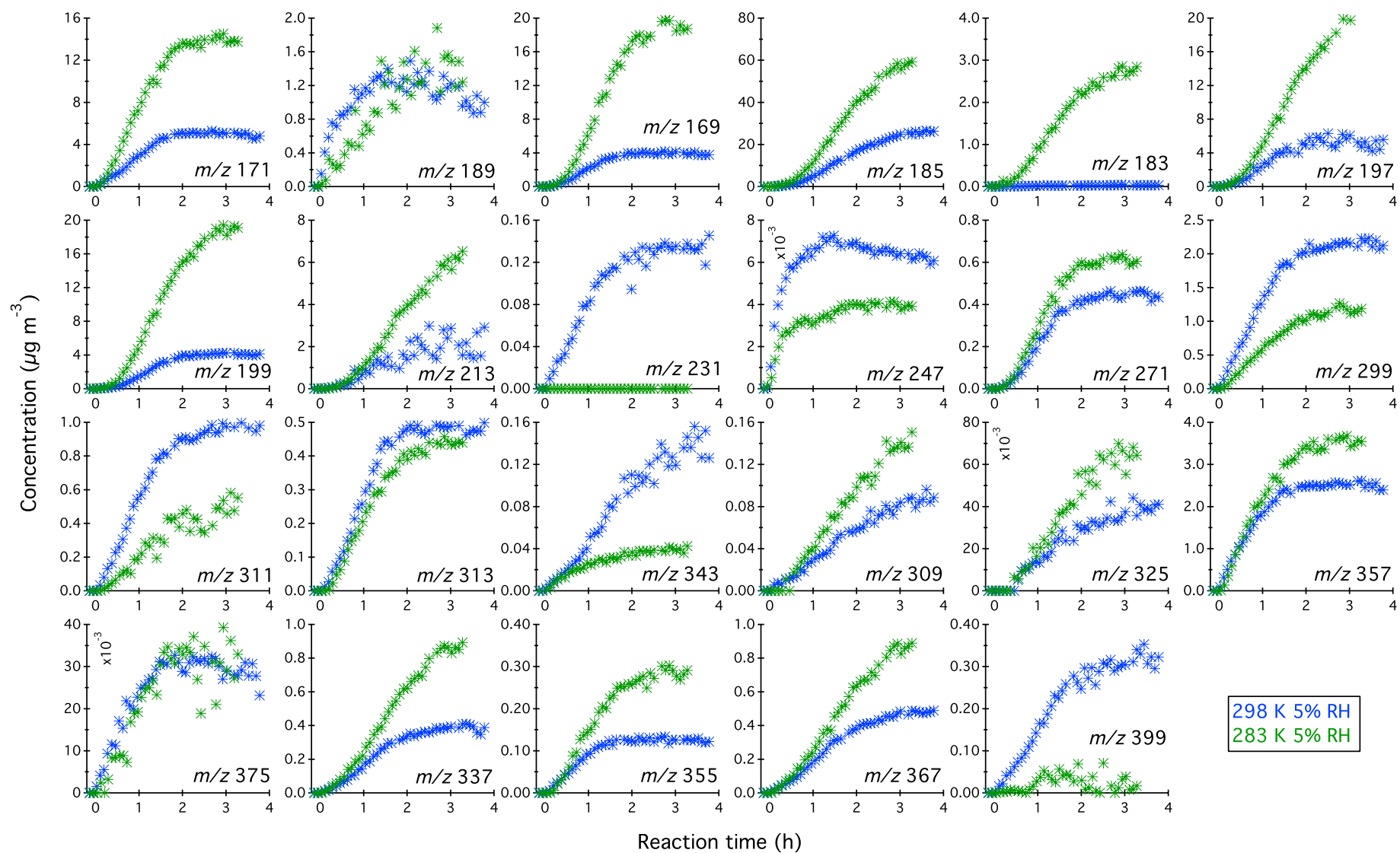


Figure S6. Temporal profiles of α -pinene+O₃ products in the particle phase: temperature effect.

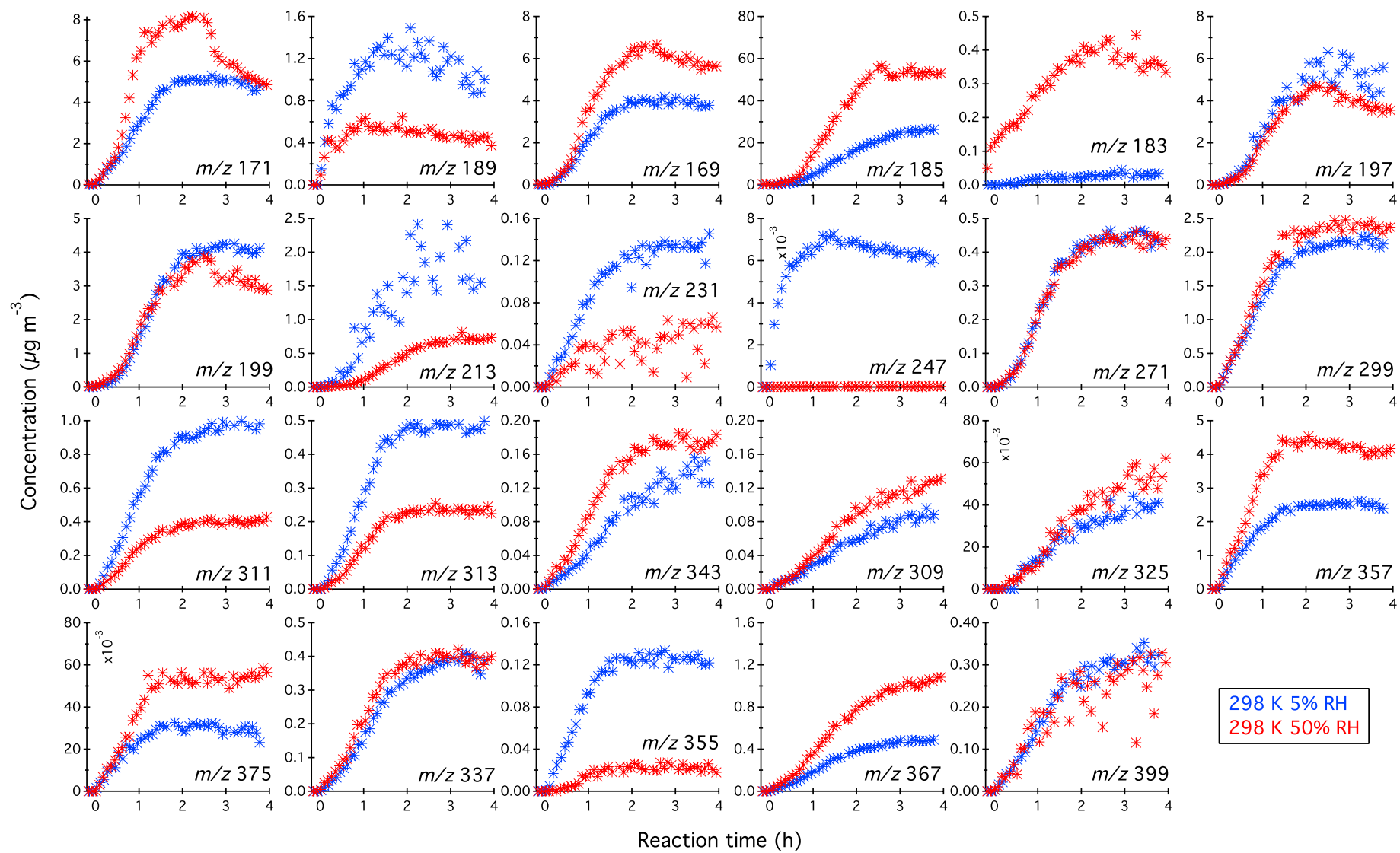


Figure S7. Temporal profiles of α -pinene+O₃ products in the particle phase: relative humidity effect.

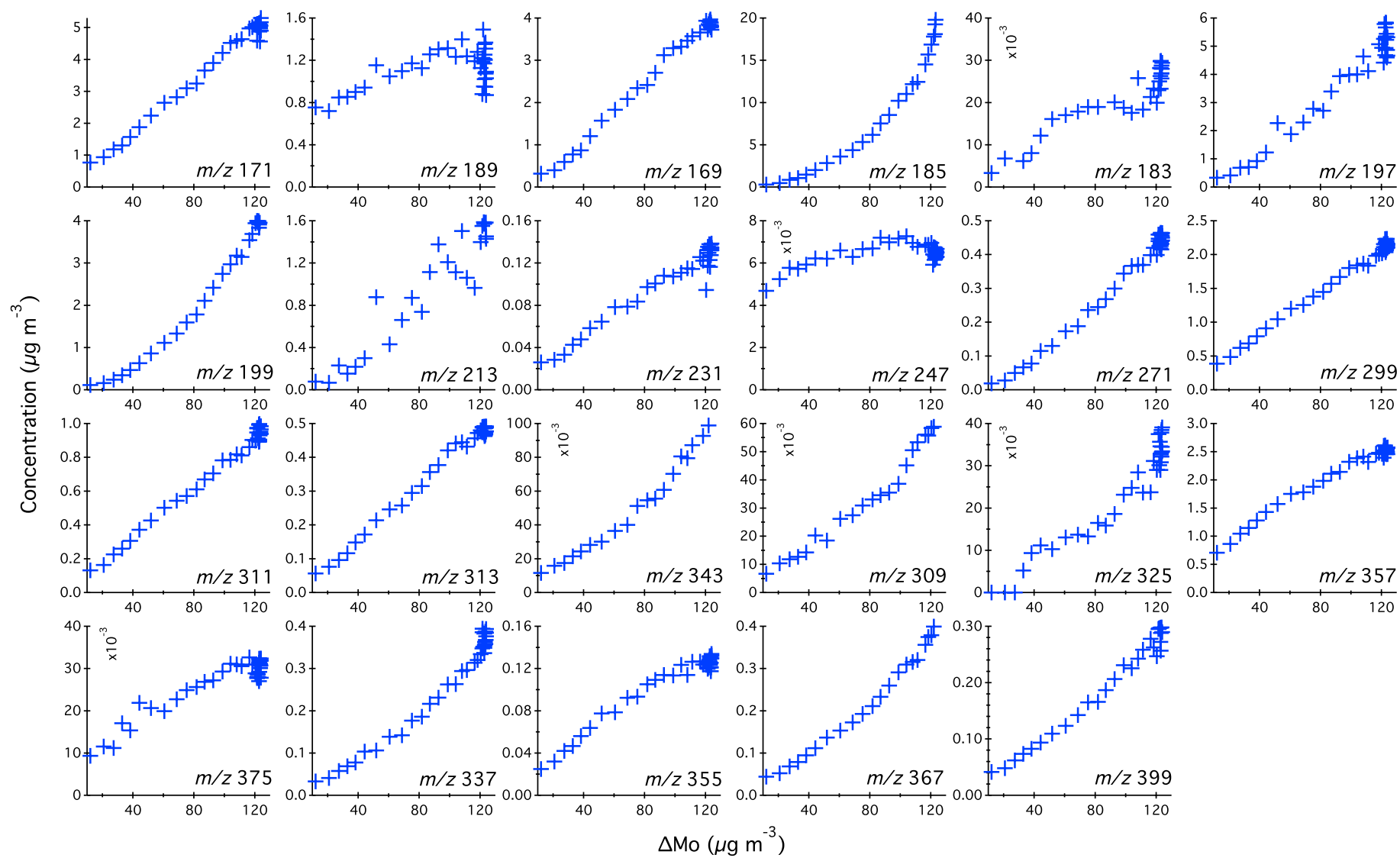


Figure S8. Temporal profiles of α -pinene+O₃ products in the particle phase as a function of total SOA mass.

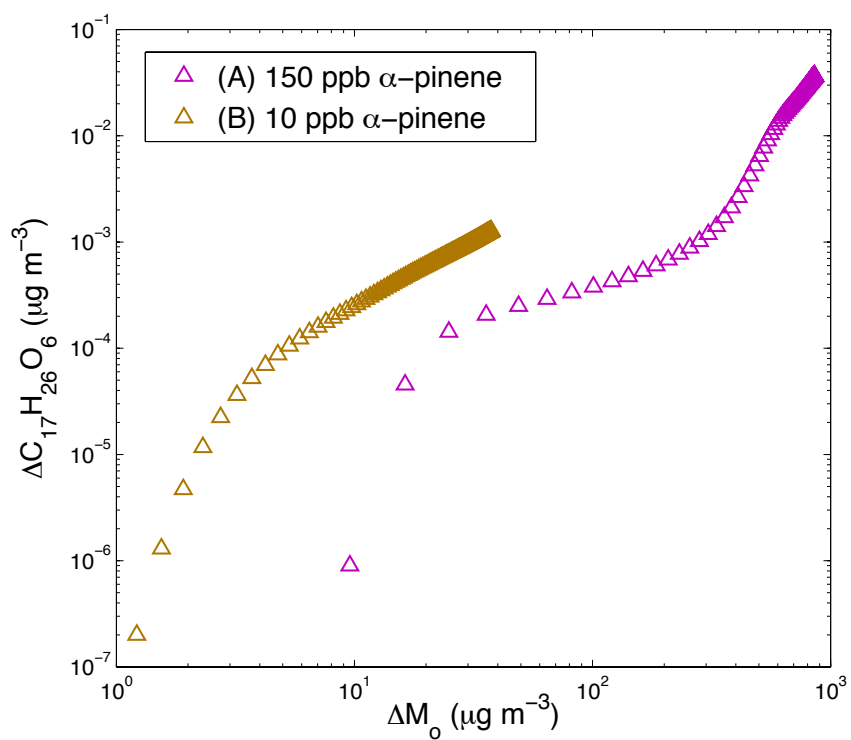


Figure S9. Simulated growth of the $C_{17}H_{26}O_6$ ester dimer in the particle phase under different initial conditions: (A) 150 ppb α -pinene + 200 ppb O_3 and (B) 10 ppb α -pinene + 20 ppb O_3 .

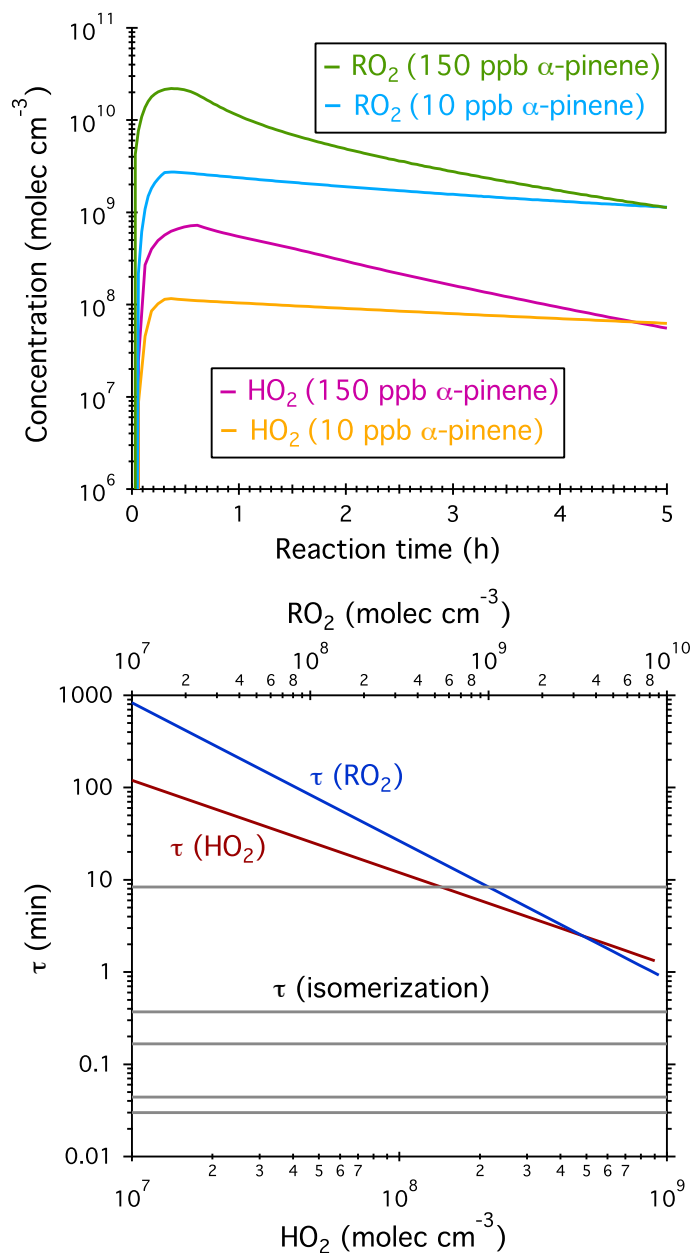


Figure S10. (Upper panel) GECKO-A simulated concentration profiles of RO₂ and HO₂ radicals under initial conditions of 150 ppb α-pinene + 200 ppb O₃ and 10 ppb α-pinene + 20 ppb O₃, respectively. (Lower panel) Estimated lifetimes of RO₂ radical with respect to self/cross combination with RO₂, reaction with HO₂, and H-shift isomerization. The RO₂+RO₂ and RO₂+HO₂ reaction rate constants are obtained from *SI Appendix, Table S4*. The isomerization reaction rate constants are from Crouse et al. (35) and Rissanen et al. (36). It can be seen that by increasing the initial α-pinene mixing ratio from 10 ppb to 150 ppb, the peak RO₂ and HO₂

concentrations are ~ 9.6 and 5.5 times higher, respectively. The corresponding lifetime of RO_2 with respect to reactions with RO_2/HO_2 decrease by less than an order of magnitude. This change is not sufficient to perturb the dynamics of overall RO_2 chemistry. In other words, the RO_2 isomerization channel is not completely shut down when α -pinene increases from 10 ppb to 150 ppb.

Table S1. Summary of experimental conditions.

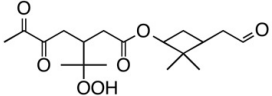
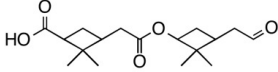
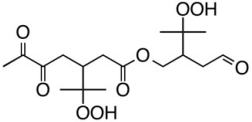
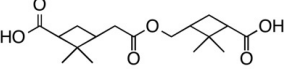
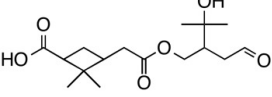
Exp. #	T ₀ (K)	RH ₀ (%)	[HC] ₀ (ppb)	[NO _x] ₀ (ppb)	[O ₃] ₀ (ppb)	Oxidants	Seed Aerosol	Initial Seed vol. (μm ³ cm ⁻³)	Maximum SOA yield ^b
1	298±2	< 5	154	< DL ^a	~ 200	O ₃	(NH ₄) ₂ SO ₄ Neutral/Dry	73	0.16
2	285±2	< 5	154	< DL	~ 200	O ₃	(NH ₄) ₂ SO ₄ Neutral/Dry	69	0.28
3	298±2	55±2	157	< DL	~ 200	O ₃	(NH ₄) ₂ SO ₄ Neutral/Wet	129	0.21
4	298±2	< 5	133	< DL	~ 3	OH	(NH ₄) ₂ SO ₄ Neutral/Dry	106	0.29
5	298±2	46±1	139	< DL	~ 3	OH	(NH ₄) ₂ SO ₄ Neutral/Wet	107	0.31

^a Detection limits (DL) for O₃, NO, and NO₂ are 0.5 ppb, 0.4 ppb, and 0.4 ppb, respectively. H₂O₂ has an interference on the O₃ detection, increasing the O₃ monitor readout by ~ 2-3 ppb in the current study.

^b Yield is defined as the mass of organic aerosols produced divided by the mass of hydrocarbon reacted.

Table S2. α -pinene SOA constituents measured by PILS + UPLC/ESI-Q-ToFMS. Chemical standards are available for pinonic acid ($C_{10}H_{16}O_3$). Note that symbols ‘#’ and ‘*’ denote products generated solely from α -pinene+ O_3 and α -pinene+OH reactions, respectively.

Compound (Reference)	Observed m/z (-)	RT (min)	RIE (Uncertainties)	Molecular formula (error / ppm)	Proposed structure from literatures and this study
Diaterpenylic acid (9, 12, 13, 15) #	189.0745 [M-H] ⁻	3.41	0.65 (\pm 40.29%)	$C_8H_{14}O_5$ (-9.5 ppm)	
Oxopinonic acid (6) #	197.0793 [M-H] ⁻	3.86	0.99 (\pm 45.79%)	$C_{10}H_{14}O_4$ (-10.7 ppm)	
Terpenylic acid (9, 12, 13, 15)	171.0652 [M-H] ⁻	3.96	1.32 (\pm 65.93%)	$C_8H_{12}O_4$ (-2.9 ppm)	
OH-pinonic acid (5, 6, 7, 10, 13, 15)	199.0949 [M-H] ⁻	4.07	2.49 (\pm 78.04%)	$C_{10}H_{16}O_4$ (-10.5 ppm)	
Diaterpenylic acid acetate (9, 12)	231.0907 [M-H] ⁻	4.12	4.32 (\pm 131.99%)	$C_{10}H_{16}O_6$ (-10.4 ppm)	
Pinic acid (5, 6, 7, 10, 13, 15)	185.0814 [M-H] ⁻	4.35	0.73 (\pm 41.90%)	$C_9H_{14}O_4$ (0 ppm)	
Pinalic acid (5, 6, 7, 10) #	169.0855 [M-H] ⁻	4.58	0.54 (\pm 38.62%)	$C_9H_{14}O_3$ (-5.9 ppm)	
Pinonic acid (5, 6, 7, 10, 13, 15)	183.1023 [M-H] ⁻	4.96	1.00 (1.1 ppm)	$C_{10}H_{16}O_3$ (1.1 ppm)	
Pinyl-diaterebyl ester (13, 14, 15) #	343.1364 [M-H] ⁻	5.45	5.81 (\pm 133.49%)	$C_{16}H_{24}O_8$ (-8.5 ppm)	
Pinyl-diaterpenyl ester (11, 12, 13, 14, 15) #	357.1547 [M-H] ⁻	5.32	4.19 (\pm 94.40%)	$C_{17}H_{26}O_8$ (-0.6 ppm)	
Pinonyl-pinyl ester (8, 13, 14, 15) #	367.1761 [M-H] ⁻	5.98	6.88 (\pm 162.94%)	$C_{19}H_{28}O_7$ (1.1 ppm)	
— #	213.0758 [M-H] ⁻	3.81	1.38 (\pm 51.30%)	$C_{10}H_{14}O_5$ (-2.3 ppm)	
— #	247.0633 [M-H] ⁻	4.55	375.47 (\pm 56.10%)	$C_{10}H_{16}O_5S$ (-2.8 ppm)	
Terpenyl-diaterpenyl ester #	343.1364 [M-H] ⁻	5.05	5.07 (\pm 116.51%)	$C_{16}H_{24}O_8$ (-8.5 ppm)	

— #	355.1740 [M-H] ⁻	5.62	6.69 (± 155.94%)	C ₁₈ H ₂₈ O ₇ (-4.8 ppm)	
— #	309.1708	5.70	As <i>m/z</i> 325	C ₁₇ H ₂₆ O ₅ (1.9 ppm)	
— #	299.1486 [M-H] ⁻	5.78	As <i>m/z</i> 357	C ₁₅ H ₂₄ O ₆ (-3.0 ppm)	—
— #	311.1489 [M-H] ⁻	5.80	As <i>m/z</i> 313	C ₁₆ H ₂₄ O ₆ (-1.9 ppm)	—
— #	399.1628 [M-H] ⁻	5.88	As <i>m/z</i> 343	C ₁₉ H ₂₈ O ₉ (-6.8 ppm)	—
— #	375.1654 [M-H] ⁻	5.90	7.05 (± 169.00%)	C ₁₇ H ₂₈ O ₉ (-0.3 ppm)	
— #	325.1646 [M-H] ⁻	6.01	5.58 (± 129.54%)	C ₁₇ H ₂₆ O ₆ (-1.5 ppm)	
— #	313.1622 [M-H] ⁻	6.08	51.64 (± 106.93%)	C ₁₆ H ₂₆ O ₆ (-9.3 ppm)	
— #	337.1634 [M-H] ⁻	6.19	As <i>m/z</i> 367	C ₁₈ H ₂₆ O ₆ (-5.0 ppm)	—
— #	271.1564 [M-H] ⁻	6.45	As <i>m/z</i> 325	C ₁₄ H ₂₄ O ₅ (7.0 ppm)	—

References: (5) Jenkin et al., 2000; (6) Jaoui and Kamens, 2001; (7) Ma et al., 2008; (8) Müller et al., 2008; (9) Claeys et al., 2009; (10) Camredon et al., 2010; (11) Gao et al., 2010; (12) Yasmeen et al., 2010; (13) Kristensen et al., 2013; (14) Kristensen et al., 2014; (15) Witkowski and Gierczak, 2014.

Table S3. CIMS ions that represent gas-phase products generated from ozonolysis and OH-initiated oxidation of α -pinene. Note that symbols ‘#’ and ‘*’ denote products generated solely from α -pinene+O₃ and α -pinene+OH reactions, respectively.

Molecular weight	Molecular formula	Observed m/z (-)	Proposed structure
116	C ₄ H ₄ O ₄	135 & 201	
142	C ₈ H ₁₄ O ₂	227	
146	C ₆ H ₁₀ O ₄	231	
156	C ₈ H ₁₂ O ₃	175 & 241	
	C ₉ H ₁₆ O ₂	241	
158	C ₇ H ₁₀ O ₄	243	
	C ₈ H ₁₄ O ₃	243	
		177 & 243	
168	C ₁₀ H ₁₆ O ₂	253	
170	C ₉ H ₁₄ O ₃	189 & 255	
172	C ₉ H ₁₆ O ₃	191 & 257	
		257	
174	C ₇ H ₁₀ O ₅	259	
	C ₈ H ₁₄ O ₄	259	
		193 & 259	
184	C ₁₀ H ₁₆ O ₃	203 & 269	
		269	

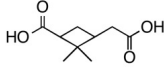
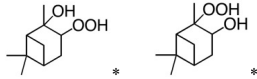
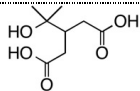
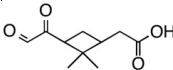
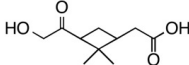
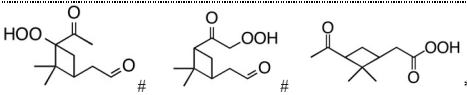
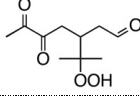
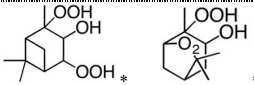
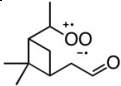
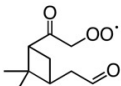
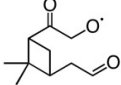
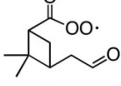
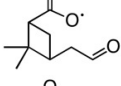
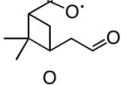
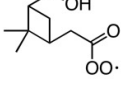
186	$C_9H_{14}O_4$	271	
188	$C_{10}H_{20}O_3$	273	
190	$C_8H_{14}O_5$	209 & 275	
198	$C_{10}H_{14}O_4$	217	
200	$C_{10}H_{16}O_4$	219 & 285	
		285	
216	$C_{10}H_{16}O_5$	301	
218	$C_{10}H_{18}O_5$	303	

Table S4. Gas- and particle-phase reactions incorporated in simulations. ‘G’ and ‘P’ denotes gas-phase and particle-phase reactions, respectively. Acronyms of each species are consistent with those used in MCMv3.2. Concentrations of OH, HO₂, and RO₂ radicals are predicted by GECKO-A using the corresponding experimental conditions (154 ppb α-pinene, 200 ppb O₃, zero NO_x, 298 K, and < 5% RH) as the input.

No.	Reactants	Products			Reaction rate constant (cm ³ molec ⁻¹ s ⁻¹)
		Name	Structure	Vapor pressure Vapor wall loss rate	
G01	APINENE + O ₃	0.6 × APINOOA		---	$6.3 \times 10^{-16} \times \exp(-580/\text{Temp})$
G02	APINENE + OH	Products	---	---	$1.2 \times 10^{-11} \times \exp(440/\text{Temp})$
G03	APINOOA	0.45 × C109O2		---	10 ⁶
G04	C109O2 + RO ₂	0.9 × C109O		---	2×10^{-12}
G05	C109O	0.8 × C89CO3		---	10 ⁶
G06	C89CO3 + HO ₂	0.44 × C89CO2		---	$5.2 \times 10^{-13} \times \exp(980/\text{Temp})$
G07	C89CO3 + RO ₂	0.7 × C89CO2		---	5×10^{-12}
G08	C89CO2	0.8 × C811CO3		---	10 ⁶
G09	C811CO3 + HO ₂	0.15 × PINIC	see Fig. 4	$9.92 \times 10^{-10} \text{ atm}$ $1.88 \times 10^{-5} \text{ s}^{-1}$	$5.2 \times 10^{-13} \times \exp(980/\text{Temp})$
G10	C811CO3 + RO ₂	0.3 × PINIC	see Fig. 4	$9.92 \times 10^{-10} \text{ atm}$ $1.88 \times 10^{-5} \text{ s}^{-1}$	5×10^{-12}
G11	2 × C811CO3	0.02 × DIACYLPER	see Fig. 4	$8.13 \times 10^{-16} \text{ atm}$ $4.36 \times 10^{-4} \text{ s}^{-1}$	5×10^{-12}
G12	PINIC + OH	Products	---	---	7.3×10^{-12}
P01	DIACYLPER	0.5 × ESTER	see Fig. 4	$2.62 \times 10^{-12} \text{ atm}$ $2.22 \times 10^{-4} \text{ s}^{-1}$	$1 \times 10^{-1} (\text{s}^{-1})$
P02	DIACYLPER	0.5 × PINIC	see Fig. 4	$9.92 \times 10^{-10} \text{ atm}$ $1.88 \times 10^{-5} \text{ s}^{-1}$	$1 \times 10^{-1} (\text{s}^{-1})$